



Comparison of systems with complex behavior

Igor Mezić^{a,*}, Andrzej Banaszuk^b

^a *Department of Mechanical and Environmental Engineering, University of California, Santa Barbara, CA 93106, USA*

^b *United Technologies Research Center, East Hartford, CT 06108, USA*

Received 17 July 2002; received in revised form 21 June 2004; accepted 21 June 2004

Communicated by C.K.R.T. Jones

Abstract

We present a formalism for comparing the asymptotic dynamics of dynamical systems with physical systems that they model based on the spectral properties of the Koopman operator. We first compare invariant measures and discuss this in terms of a “statistical Takens” theorem proved here. We also identify the need to go beyond comparing only invariant ergodic measures of systems and introduce an ergodic–theoretic treatment of a class of spectral functionals that allow for this. The formalism is extended for a class of stochastic systems: discrete Random Dynamical Systems. The ideas introduced in this paper can be used for parameter identification and model validation of driven nonlinear models with complicated behavior. As an illustration we provide an example in which we compare the asymptotic behavior of a combustion system measured experimentally with the asymptotic behavior of a class of models that have the form of a random dynamical system.

© 2004 Elsevier B.V. All rights reserved.

1. Introduction

This paper is concerned with the issue of comparison of different dynamical system models of a physical system or models of a physical system with the system itself. There are various ways of comparing the behavior of two dynamical systems. All of them involve defining a metric or convergence. Within the dynamical systems community, this led the investigation of the above issue in the direction of defining different topologies on spaces of dynamical systems. The definitions of weak and strong topologies for automorphism groups are given in [16,30]. These are based on the comparison of the action of dynamical systems on open sets of the phase space, and are effectively requirements that the two systems actions be close everywhere. For example, convergence of a sequence

* Corresponding author. Tel.: +1 805 893 7603; fax: +1 805 893 8651.

E-mail address: mezic@engineering.ucsb.edu (I. Mezić).

of automorphisms $\{T_i\}$ to T in the strong topology means that $\{T_i\}$ and T coincide on a larger and larger portion of the phase space as i increases. In the context of modeling, the requirement that the action of two dynamical systems be close everywhere is too strong. Consider, for example systems treated in statistical mechanics. The relationship $PV = RT$ is recovered by employing a model consisting of noninteracting particles in a container. This model is certainly not very close (in the sense that the dynamical action of the model on the phase space is not close) to the real dynamics of molecules of monatomic gases for some regimes. But, they possess the same *time-averaged properties*. Another situation of interest occurs when systems with (formally) infinite number of degrees of freedom are truncated using e.g. Galerkin method to obtain a finite system of ordinary differential equations. In this case, only a proper subset of the initial conditions available for the infinite-dimensional system can be propagated in time by the finite-dimensional truncation, and the comparison in the detailed sense of strong or weak topologies is not possible. These considerations naturally lead to the study of asymptotic dynamics of selected trajectories and this approach was taken in [4], where the emphasis is on comparing invariant measures. In the case when one of the two systems has a smaller space of initial conditions than the other (e.g. Galerkin projections), projection of invariant measures is used. The approach that we pursue here is related to the method of comparison of time series espoused by Moeckel and Murray [29]. In fact, the first part of this paper in which we deal with invariant measures, connects directly to that paper and clarifies some issues regarding ergodic–theoretic properties of the approach in [29] and its relationship with the Takens theorem. While in numerical experiments and analytical work the full state of a system is an observable, in experiments this is typically not the case. Usually the value of one observable – a function on the phase space – is measured. This observation lead to the development of the Takens embedding theorem [38], that was followed by a large number of works in which the theorem was used to illuminate *topological properties* of experimental data sets [1]. As far as *statistical properties* of data are concerned, Takens embedding theorem has been used by Mischaikow et al. [28] to identify symbolic dynamics from experimental time series. In the prior work of Froyland et al. [13] a suggestion is made on getting invariant measures from data (upon embedding the data using Takens theorem) using representation of the dynamical system as a random system, triangulating the data and assigning weight to each triangular section according to the properties of the associated random system. The motivation in [13] is that there are many problems in which the length of signal in time is not sufficient to perform averaging operations and compute statistics. However, there are a variety of problems in which long data traces are available, and we develop here a direct approach using time averages of functions, which can be associated with eigenfunctions of the Koopman operator [20,30] of the dynamical system at hand. In order to pursue this, we need to prove (*constructively*) that ergodic partitions and invariant measures of systems can be compared using a single observable. This leads to what we call the statistical Takens theorem (**Theorem 2**). Using this result, we develop pseudometrics on spaces of dynamical systems allowing us to compare asymptotic dynamics of systems.

In some contexts though, comparing invariant measures is not enough. Consider, for example two systems that have a (geometrically) identical globally attracting limit cycle, but on the limit cycle of the first system the dynamics is given by $\dot{\theta} = \omega_1$ and on the limit cycle of the second system the dynamics is given by $\dot{\theta} = \omega_2$, where $\omega_1 \neq \omega_2$. While these two systems have identical invariant measures supported on the same geometrical object, their *asymptotic speed* is different. This is related to the description of the cycling behavior of dynamical systems, the study of which was pursued by Dellnitz and Junge [11]. In that work, the formalism is based on the Perron–Frobenius operator of the associated stochastic systems. In their work, the concept of eigenmeasures, extending the idea of invariant measures, is introduced. In examples that Dellnitz and Junge treat stochasticity is associated with the round-off truncation in the computation of deterministic dynamical systems. In [8], Perron–Frobenius operator is also analyzed from the spectral perspective. We propose here an alternative formalism based on harmonic analysis of the Koopman operator that extends the concept of comparing the invariant measures using time-averages. The regularity results allowing us to do this in the context of deterministic systems are contained in [41]. We show that information beyond that obtained using time averages can be acquired by taking harmonic averages if the system has a *factor* that is a rotation on a circle. The relationship between spectrum at eigenvalue 1 and invariant measures on the phase space is extended by associating complex measures (constructed explicitly using the Riesz representation theorem) with eigenvalues of the form $e^{-i2\pi\omega}$ for $\omega \neq 0$.

As pointed out above, both the concepts of invariant measure and the harmonic average formalism developed here are related to spectral properties (in particular, the point spectrum) of the so-called Koopman operator U , a linear operator that acts on functions on the phase-space [20,30]. We stress that in this context questions of identification or validation of asymptotic properties of nonlinear finite-dimensional systems with complex dynamics is transferred to questions of identification or validation of a linear, albeit infinite-dimensional Koopman operator. Our hope is that some of the methods developed in control theory of linear systems can be used to study these issues further (for a combination of linear system identification procedures with dynamical systems analysis, see [14]). In addition, there has been a substantial interest recently in improving the Galerkin projection methods for obtaining low-dimensional models of formally infinite-dimensional systems by introducing stochastic terms to account for neglected modes [15,6,39,31,3,23,7]. A dynamical systems perspective on such modelling is provided in the work of Dellnitz and collaborators [11,10] in the context of Perron–Frobenius operator for stochastic systems. Here, we develop a formalism for stochastic systems in the context of Koopman operator akin to that of deterministic systems that allows for a systematic comparison of different models or data with stochastic elements. In this extension of the deterministic theory we study deterministic factors of stochastic systems – a concept that might help in understanding e.g. the abundance of oscillatory phenomena on various time-scales in climate dynamics (see e.g. [33]). The example of experimental data analysis and comparison with models is given towards the end of the paper. The data – experimental data from a combustion rig – has stochastic features and the models are random dynamical systems. Our methods allow for model parameter identification in this context. They also allow for an easy distinction between processes having a deterministic factor on a circle (deterministic limit cycling) with additive noise, and lightly damped but stable (i.e. deterministic factor has a fixed point) process – a question that received some interest in the literature [22,17].

The paper is organized as follows: in Section 2, we discuss the relationship between invariant measures and time averages of a certain set of functions on the phase space. Extending the ideas in [25,27]. Based on this we discuss different pseudometrics on the space of dynamical systems that split that space into equivalence sets of system having the same (according to the chosen pseudometric) asymptotic dynamics and we present some examples showing both the strength and the weaknesses of the method. To remedy the weaknesses, in Section 3 we turn to analyzing the spectral properties of observables of a dynamical system, by introducing a class of functionals on trajectories (or equivalently, a class of operators on functions induced by the dynamical system) of which the time-averaging functional is a member. Spectral properties are discussed and methods for comparing spectra introduced. In Section 4, we extend these ideas to a specific class of stochastic systems, discrete Random Dynamical Systems. In Section 5, an example of using the theory to model and analyze an experimental combustion system is presented. Optimization of the model parameters is attempted using the ideas on comparing asymptotic dynamics described in Sections 2–4. Proofs of some of the main theoretical results are provided in the Appendix A.1.

2. Comparison of long-term dynamics: ergodic partitions and invariant measures

2.1. Invariant measures from a single variable

We consider a dynamical system in discrete time defined by

$$x_{i+1} = T(x_i), \quad y_i = f(x_i), \quad (1)$$

where $i \in \mathbb{Z}$, $x_i \in M$, $T : M \rightarrow M$ is measurable and f is a smooth real function on a compact Riemannian manifold M endowed with the Borel sigma algebra. Every continuous dynamical system on a compact manifold possesses

an invariant measure μ . We call the function f^* the time average of a function f under T if

$$f^*(x) = \lim_{n \rightarrow \infty} \frac{1}{n} \sum_{i=0}^{n-1} f(T^i x)$$

almost everywhere (a.e.) with respect to the measure μ on M . The time average f^* is a function of the initial state x . The operator $P_T : L^1 \rightarrow L^1$ such that $P_T(f) = f^*$ is called the time-averaging operator. Note that by Birkhoff’s pointwise ergodic theorem [30], if T is measure-preserving, f^* exists for every function $f \in L^1(M)$.

A partition ζ of M is defined to be a collection of disjoint sets D_α^ζ , where α is some indexing set, such that $\mu(\cup_\alpha D_\alpha^\zeta) = \mu(M)$ (see [32]). A product $\zeta \vee \lambda$ of two partitions ζ, λ is a partition into sets $D_{(\alpha,\beta)}^{\zeta \vee \lambda} = D_\alpha^\zeta \cap D_\beta^\lambda$ i.e. sets that are intersections of elements of the two partitions. For a finite or countable product ζ of partitions ζ_i , we write $\zeta = \bigvee_i \zeta_i$. The key object in our considerations is partition of the phase space into sets on which the time-averages are constant, i.e. into level sets of f^* . In particular, let f be a continuous function on M . The family of sets $C_\alpha, \alpha \in \mathbb{R}$ such that $C_\alpha = (f^*)^{-1}(\alpha)$ is a (measurable) partition of M . We denote this partition by ζ_f and call it the *partition induced by f* .

Every partition ζ_f splits the phase space into sets on which the time-average of f is constant. It turns out that for continuous f the measure zero set on which f^* is not defined is independent of f [24] when M is a compact metric space. An important partition associated with a dynamical system T is its *ergodic partition*: partition of the phase space into (invariant) sets on which T is ergodic (for a precise definition, see the [Appendix A.1](#)). Intuitively, if we pick a set in the ergodic partition, the system will sample that set well on almost every trajectory in the set.

Example 1. Let $I = [-1, 1]$. Consider the (non-invertible) map $T : I \rightarrow I$, defined by $T(x) = 2x, \pmod{[-1, 1]}$ (see [Fig. 1](#)) that preserves the Lebesgue measure (line length) on the interval I . Clearly, $D_1 = (0, 1]$ and $D_2 = [-1, 0)$ are invariant sets. The map restricted to each of these sets is ergodic. The ergodic partition is $\zeta = \{D_1, D_2\}$. Note that ergodic partition is defined up to measure zero: thus we did not need to include the fixed point 0 in the ergodic partition.

Our goal is to use time averages obtained from a *single observable* to construct the ergodic partition and thus allow for reconstruction of the ergodic partition from experiments (note however that if there is more than one set in the ergodic partition, we will need to sample that observable from more than one initial condition, as should be clear from [Example 1](#)).

Theorem 2. Let M be a compact Riemannian manifold of dimension m . Let $l/2 > |f|$ and $\kappa_i, i \in \mathbb{N}^+$ a sequence of continuous periodic functions in $C([-l/2, l/2])$ that is complete. Consider a countable set of functions $f_{i_1, \dots, i_{2m+1}} =$

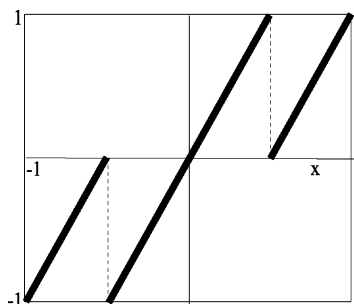


Fig. 1. The map considered in Example 1.

$\kappa_{i_1}(f) \cdot \kappa_{i_2}(f \circ T) \cdot \dots \cdot \kappa_{i_{2m+1}}(f \circ T^{2m})$ (where $i_1, i_2, \dots, i_{2m+1} \in \mathbb{N}^+$). Then, for $C^r, r \geq 1$ pairs (f, T) it is a generic property that the ergodic partition of a dynamical system T on M is

$$\zeta_e = \bigvee_{i_1, \dots, i_{2m+1}} \zeta_{f_{i_1, \dots, i_{2m+1}}}.$$

The proof is provided in the [Appendix A.1](#), and it relies on two lemmas. The first one extends an argument in ergodic theory which says that the ergodic partition is partition into joint level sets of time averages of a countable, dense set of continuous functions (for the proof and applications see [\[25,27\]](#)) to allow for taking only joint level sets of time averages of a complete set of functions. The second lemma tells us how to generate such a complete set of functions using only one observable. The essence of the above result is the following. By Takens theorem, we know that we can embed the signal $f(T^j), j \in \mathbb{Z}^+$ of a continuous observable f of a system T into an $2m + 1$ dimensional box \mathbb{B} of side l , where $|f| < l/2$. We prove ([Appendix A.1, Lemma 20](#)) that to find the ergodic partition we only need to exhibit a dense countable subset of continuous functions. Such a subset is going to be provided by products of compositions of $(2m + 1)$ –products of complete set of continuous periodic functions on \mathbb{R} of period l with a generic observable f , i.e. we only need to compute the time-averages of functions

$$\kappa_{i_1}(f(x)) \cdot \kappa_{i_2}(f \circ T(x)) \cdot \dots \cdot \kappa_{i_{2m+1}}(f \circ T^{2m}(x)).$$

Example 3. The set of products of functions $\sin((2\pi/l)ny), \cos((2\pi/l)ky), (1/2), y \in \mathbb{R}, k, e, n \in \mathbb{N}^+$ is a complete set in $C(\mathbb{B})$. If $m = 1$ (i.e. the embedding dimension is 3), we should compute time averages of products

$$f_1\left(\frac{2\pi}{l}nf(T^2x)\right) f_2\left(\frac{2\pi}{l}kf(Tx)\right) f_3\left(\frac{2\pi}{l}jf(x)\right),$$

where $f_i(z) = \sin(z)$, or $\cos(z)$ and $k, n, j \in \mathbb{N}^+$.

Example 4. [Theorem 2](#) can be used to identify invariant sets (and ultimately the ergodic partition) of a system without measuring all of its variables for all time. All that is needed is knowledge of initial conditions and knowledge of a single variable time trace. Consider the standard map on a torus, given by

$$\left. \begin{aligned} I' &= I + \epsilon \sin(2\pi\theta), \\ \theta' &= \theta + I + \epsilon \sin(2\pi\theta), \end{aligned} \right\} \text{mod } 1. \tag{2}$$

Physically, this can be derived as a Poincaré map of a plane pendulum kicked periodically with an impulsive force. Assume that we know the initial conditions: the action I and the angle θ , but we can only measure θ dynamically. [Theorem 2](#) suggests that we can find the ergodic partition from these measurements. In [Fig. 2a](#) we show contour plot visualizing the level sets of finite time average $f_1^{*,N} + f_2^{*,N} + f_3^{*,N} + f_4^{*,N}$, where

$$f_1^{*,N} = \frac{1}{N} \sum_{j=1}^N \sin(2\pi\theta^j) \sin(2\pi\theta^{j-1}),$$

$$f_2^{*,N} = \frac{1}{N} \sum_{j=1}^N \sin(2\pi 3\theta^j) \cos(2\pi 3\theta^{j-1}),$$

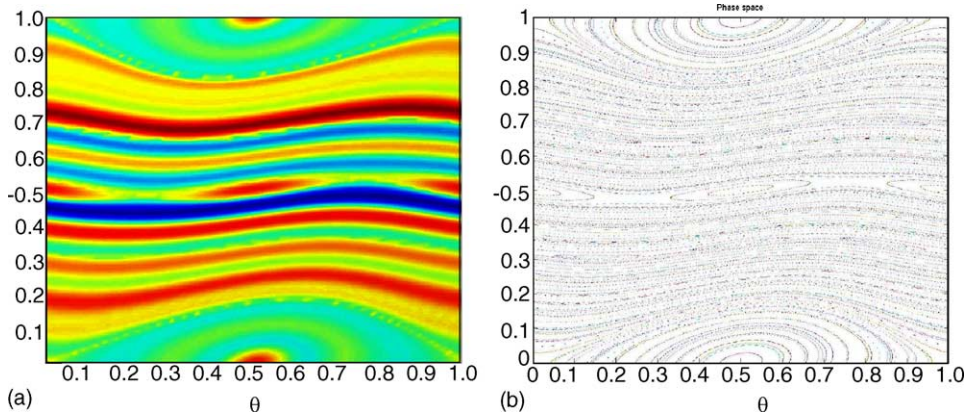


Fig. 2. (a) Contour plot showing the level sets of $f_1^{*,N} + f_2^{*,N} + f_3^{*,N} + f_4^{*,N}$. Simulation for $N = 100$ iterates, 10,000 initial conditions on a regular 100×100 grid. The parameter $\epsilon = 0.03$. (b) Phase space plot of the standard map for 400 initial conditions on a regular 20×20 grid. The parameter $\epsilon = 0.03$.

$$f_3^{*,N} = \frac{1}{N} \sum_{j=1}^N \sin(2\pi 5\theta^j) \cos(2\pi 5\theta^{j-1}),$$

$$f_4^{*,N} = \frac{1}{N} \sum_{j=1}^N \cos(2\pi 8\theta^j) \sin(2\pi 8\theta^{j-1}),$$

Note that joint level sets of f_1^* , f_2^* , f_3^* , f_4^* are not equivalent to level sets of $f_1^* + f_2^* + f_3^* + f_4^*$ – in particular two different joint level sets of f_1^* , f_2^* , f_3^* , f_4^* might be subsumed into a single level set of the sum, but we get reasonable results visualizing joint level sets this way. The problem of visually depicting joint level sets of many functions is not a simple one (it goes under the name of image segmentation in computer science). Simulation in Fig. 2a was performed for $N = 100$ iterates, 10,000 initial conditions on a regular 100×100 grid. Simulation in Fig. 2b shows the usual representation of the phase-space trajectories and was performed for 100 iterates, 400 initial conditions on a regular 20×20 grid. Both figures were obtained for $\epsilon = 0.03$. The contour plot, that was calculated by taking time averages of observables according to prescription in Theorem 2 shows close resemblance to the phase portrait. For our test functions f_1 , f_2 , f_3 , f_4 we chose some of the products suggested in the previous example. Note that we have embedded the time-traces into a box $[0, 1] \times [0, 1] \subset \mathbb{R}^2$ by observing that θ is defined mod 1. Also note that, since we know the dimension m of the phase space in this example, we did not embed the signal in \mathbb{R}^{2m+1} , but in \mathbb{R}^m .

As the above example shows, the ideas in Theorem 2 allow for visualization of structures in the phase space of a system even if only a single variable can be measured dynamically (but we have knowledge of initial conditions). This might be particularly important for conservative systems such as the one treated in Example 4. Even if initial conditions are known only on a subset of the phase space (such as in numerical simulation of partial differential equations, where, due to the vast phase space it is impossible to obtain results for a large set of initial conditions), application of these ideas will lead to splitting initial conditions into equivalence classes that possess the same asymptotic dynamics (in the sense of invariant measures).

The same result as stated in Theorem 2 holds for systems not defined on compact spaces, but whose attractors are compact sets that are not necessarily manifolds. The extension of Takens theorem for this case can be found in [34].

2.2. Pseudometrics

According to the above description, the asymptotic dynamics partitions the phase space into invariant sets. A sequence of numbers $f_{i_1, \dots, i_{2m+1}}^*$ is associated with each set in the partition. We can base different pseudometrics on spaces of dynamical systems by using the partition. Let μ be a Borel measure on the compact metric space M . We are going to call systems for which f^* exists for every $f \in L^1(M)$ \mathcal{B} -regular [9]. We could use time averages to distinguish between systems: e.g. let T_1 and T_2 be two continuous, \mathcal{B} -regular transformations on M . Then, we could use

$$d^a(T_1, T_2) = \max_{f \in C(M)} \frac{|P_{T_1}(f) - P_{T_2}(f)|}{|f|}, \tag{3}$$

an “asymptotic pseudodistance” between T_1 and T_2 , where $|f|$ can be any suitable function norm, e.g. L^1 norm.

Example 5. Consider $T_1, T_2 : \mathbb{R}^2 \rightarrow \mathbb{R}^2$ for which all trajectories tend to $S^1 \in \mathbb{R}^2$ but the dynamics of $T_{1,2}$ on S^1 is given by $\theta \rightarrow \theta + \alpha_{1,2}$, where both α_1 and α_2 are irrational and the map is mod 1. The pseudodistance $d^a(T_1, T_2) = 0$. On the other hand, if α_2 is rational, the pseudodistance is nonzero.

Thus, even (3) might not be too useful for comparing the statistics: on one hand it does not distinguish between the systems having very different dynamics but equal statistics like in the [Example 5](#), and on the other hand it distinguishes between the systems described in the following example:

Example 6. Let $T_1 : x_1^{i+1} = \lambda x_1^i$ and $T_{2m} : x_2^{i+1} = \lambda(x_2^i - \epsilon_m) + \epsilon_m$, where $x_1, x_2 \in [-1, 1]$, $|\epsilon_m| < 1$ and $0 < \lambda < 1$. The first system has an asymptotically stable fixed point at $x_1 = 0$ and the second one at $x_2 = \epsilon_m$. The pseudodistance $d^a(T_1, T_{2m}) > a > 0$ for $\epsilon_m = 1/m$ (i.e. a is a lower bound on the pseudodistance) as there exists a continuous function f with arbitrarily small L^1 norm on $[-1, 1]$ that is zero at zero and equal to any given value at ϵ .

As shown in the above example, two systems that have attractors that are very close in space can be distant according to d^a . Thus, we come to the point where we define a very natural distance between two systems when we are only interested in matching the asymptotic dynamics on some scale: choose a finite number of functions (i.e. introduce a cut-off) on the phase space and compare the statistics on those. The pseudodistance between T_1, T_2 relative to a function $f : M \rightarrow \mathbb{R}$ is defined as

$$d_f^a(T_1, T_2) = \frac{|P_{T_1}(f) - P_{T_2}(f)|}{|f|}, \tag{4}$$

The most important property of d_f^a that it renders systems that have “close” attractors “close”. In [Example 6](#), making ϵ_m smaller would make T_{2m}^m converge to T_1 in d_f^a for any smooth f . Obviously, the sum of any number of pseudometrics is a pseudometric. In a specific problem, it is typically easy to identify the important f 's. In our thermodynamic example from the introduction it can be the energy of the system. In the case of oscillators, it will be the amplitude of oscillation, etc. In [29] various types of pseudometrics are discussed for a particular choice of functions f that are compositions of indicator functions on “box” sets in indicator space with time-delay embedded observable. We use such functions in our application [Section 5](#).

The pseudometrics of type (4) are still not entirely satisfactory, as they lose all the “timescale” information about the system. For example, all the irrational rotations on the circle are again identified, as in [Example 5](#). To treat this problem, we need to extend our formalism to include spectral information.

3. Comparison of long-term dynamics: harmonic analysis

We pointed out in the introduction that two systems that have equal statistics in the sense of invariant measures, can have very different asymptotic dynamics. We provided the following example (here in discrete time): consider

two systems that have a (geometrically) identical global attractor which is a circle, but on the attractor of the first system the dynamics is given by $\theta' = \theta + \omega_1 \pmod{1}$ and on the attractor of the second system the dynamics is given by $\theta' = \theta + \omega_2 \pmod{1}$, where $\omega_1 \neq \omega_2$ and both frequencies are irrational. While these two systems have identical invariant measures supported on the same geometrical object, their *asymptotic speed* is different. Clearly, this has to do with the spectral properties of the two systems, and in particular with asymptotic spectral properties.

In the previous section, we have introduced the operator $P_T : f \rightarrow f^*$. Note that f^* is an eigenfunction corresponding to eigenvalue 1 of the so-called Koopman operator $U : L^1 \rightarrow L^1$, which is defined by

$$Uf(x) = f \circ T(x),$$

as f^* is constant on orbits i.e. $Uf^*(x) = f^*(x)$. The operator P_T can be considered as a member of a family of operators P_T^ω ,

$$[P_T^\omega(f)](x) = f_\omega^*(x) = \lim_{n \rightarrow \infty} \frac{1}{n} \sum_{j=0}^{n-1} e^{i2\pi j\omega} f(T^j(x)),$$

where $\omega \in [-0.5, 0.5)$. Note that $P_T = P_T^0$ and $f(T^j(x))$ is the time series of the observable f on the trajectory of the system T starting at the point x at time 0. Thus, for fixed x , $f_\omega^*(x)$ is just the Fourier transform of this time series, and it is simple to calculate using FFT. In this section, we will discuss the dynamical meaning of the spatial dependence of these Fourier transforms.

Example 7. Consider the maps $T_1, T_2 : \mathbb{R}^2 \rightarrow \mathbb{R}^2$ for which all trajectories tend to $S^1 \in \mathbb{R}^2$ but the dynamics of $T_{1,2}$ on S^1 is given by $\theta' = \theta + \alpha_{1,2}$, where both α_1 and α_2 are irrational. The pseudodistance $d_f^a(T_1, T_2) = 0$ for any continuous (or even L^1 function f). In this case, $P_{T_1}^\omega(e^{i2\pi\theta}) = 0$ for all $\omega \in S^1$, $\omega \neq -\alpha_1$, while $P_{T_2}^\omega(e^{i2\pi\theta}) = 0$ for all $\omega \in S^1$, $\omega \neq -\alpha_2$.

Like the time-averages, the functions f_ω^* also play an important role in the spectral analysis of U : they are the eigenfunctions associated with eigenvalues $e^{-i2\pi\omega}$ [30]:

$$Uf_\omega^*(x) = \lim_{n \rightarrow \infty} \frac{1}{n} \sum_{j=0}^{n-1} e^{i2\pi j\omega} f(T^{j+1}(x)) = e^{-i2\pi\omega} \lim_{n \rightarrow \infty} \frac{1}{n} \sum_{j=0}^{n-1} e^{i2\pi(j+1)\omega} f(T^{j+1}(x)) = e^{-i2\pi\omega} f_\omega^*(x).$$

It is easy to deduce using methods in [41] that existence of these averages is true for all \mathcal{B} -regular T 's, as the existence of harmonic averages depends only on the existence of certain autocorrelations which in turn depends on the existence of time-averages of functions. P_T^ω is nonzero only on at most a countable set of ω 's (Lemma in Section 4 of [41]). But, when it is non-zero, it can provide substantial new information about the process that we are studying.

It is easy to show that eigenfunctions of U can only be of the form f_ω^* . In fact, a nonzero P_T^ω is the orthogonal projection operator onto the eigenspace of U associated with the eigenvalue $e^{-i2\pi\omega}$ (see the first remark on pg. 215 in [42]). In the case of $P_T^0 = P_T$ the theory of invariant measures provides a connection of objects defined on the phase space M with the properties of P_T . In the next section we provide such a connection for P_T^ω by showing that it is associated with certain complex measures on M . We characterize these complex measures for an ergodic transformation in terms of its ergodic measure and the eigenvalues of the associated Perron–Frobenius operator and provide an example where the eigenvalues and eigenfunctions of a map which has both point and continuous spectrum are numerically computed.

3.1. Harmonic analysis and factor maps

We turn to the case when there are eigenfunctions of U that are associated with complex eigenvalues of an ergodic transformation $T : A \rightarrow A$, where $A \subset M$. In the following we relate these eigenfunctions with rotating factors of the map T . Recall that existence of a factor $S : B \rightarrow B$ of T on $A \subset M$ is established by proving that there is a measurable factor map $F : A \rightarrow B$ such that $F \circ T = S \circ F$ a.e. and $\mu(F^{-1}(E)) = \nu(E)$ for all measurable $E \subset B$, and measures μ, ν , where T preserves μ and S preserves ν . We have the following

Proposition 8. *Let $h_\omega : A \rightarrow \mathbb{C}$ be a non-constant eigenfunction of U associated with the eigenvalue $e^{-i2\pi\omega}$. Then h_ω is a factor map and T has a factor that is a rotation on a circle by angle $2\pi\omega$. Conversely, if T admits a factor map to rotation on the circle by angle $2\pi\omega$ then there is an eigenfunction of U associated with eigenvalue $e^{-i2\pi\omega}$.*

Proof. First observe that the modulus of h_ω is constant on trajectories: $|h_\omega| \circ T = |h_\omega \circ T| = |e^{-i2\pi\omega} h_\omega| = |h_\omega|$. Thus, the modulus of h_ω is constant a.e. as T is ergodic on A . Without loss of generality we assume that $|h_\omega| = 1$. Define $\theta(x)$ by $h_\omega(x) = e^{-i2\pi\theta(x)}$. We have

$$h_\omega(Tx) = e^{-i2\pi\theta(Tx)} = e^{-i2\pi\omega} h_\omega(x) = e^{-i2\pi\omega} e^{-i2\pi\theta(x)} = e^{-i2\pi(\theta(x)+\omega)}. \quad (5)$$

Thus, it is clear that $\theta(Tx) = \theta(x) + \omega$ i.e. $h_\omega \circ T = S \circ h_\omega$ where S the clockwise rotation by angle $2\pi\omega$ on the circle of radius 1. Now define a measure ν on the circle by $\nu(E) = \mu(h_\omega^{-1}(E))$ where μ is the ergodic measure for T , and E is a Borel set. We get

$$\begin{aligned} \nu(S^{-1}(E)) &= \mu(h_\omega^{-1}(S^{-1}(E))) = \mu((S \circ h_\omega)^{-1}(E)) = \mu((h_\omega \circ T)^{-1}(E)) = \mu(T^{-1}(h_\omega^{-1}(E))) \\ &= \mu(h_\omega^{-1}(E)) = \nu(E). \end{aligned}$$

ν is invariant under S and we are done with the first part of the claim. The converse is clear by the following construction: let $\eta : M \rightarrow S^1$ be a factor map of T such that

$$\eta(Tx) - \eta(x) = \omega,$$

i.e. η maps T to a rotation on the circle by an angle $2\pi\omega$. Then let

$$h(Tx) = e^{-i2\pi\eta(Tx)} = e^{-i2\pi(\eta(x)+\omega)} = e^{-i2\pi\omega} e^{-i2\pi\eta(x)} = e^{-i2\pi\omega} h(x)$$

and h is an eigenfunction associated with eigenvalue $e^{-i2\pi\omega}$. □

Corollary 9. *Let A be a set in the ergodic partition of T . $P_T^\omega(f)$ is not constant (zero) on A for every $f : M \rightarrow \mathbb{C}$ if and only if T has a factor that is a rotation on the circle by an angle $2\pi\omega$.*

These results turn our attention to the more detailed study of eigenfunctions associated with complex eigenvalues. Before we do that let us present an example of a map with a periodic factor.

Example 10. Consider a map T on the interval $I = [-1, 1]$ such that $T = -(2x) \bmod [-1, 1]$ (see Fig. 3). At every step, every point in $[0, 1]$ is mapped into $[-1, 0]$ and vice versa. Thus, the map F from I to the circle of radius 1 in the complex plane defined by $F(x) = e^{-i2\pi} = 1$ for $x \in [0, 1]$ and $F(x) = e^{-i\pi} = -1$ for $x \in [-1, 0]$ is a factor map. The factor is rotation on the circle by angle π i.e. frequency $1/2$. Clearly, if $F(x) = e^{-i\pi} = -1$ then $F(Tx) = e^{-i2\pi} = 1$ and if $F(x) = e^{-i2\pi} = 1$ then $F(Tx) = e^{-i\pi} = -1$. So $F(Tx) = e^{-i\pi} F(x)$ and F is an eigenfunction associated with frequency $\omega = 1/2$. Note that the second iterate of the map $T^2 = 4x \bmod 1$ on $(0, 1]$ and $T^2 = 4x \bmod (-1)$ on $[-1, 0)$ so the map is ergodic on I with respect to the Lebesgue measure. However, if we could only measure the observable $\text{Re}(F) : I \rightarrow \mathbb{R}$ the behavior we would measure would be pure cycling from -1 to 1 . Note that F can also be considered as a map on $S^0 = \{-1, 1\}$ instead on S^1 .

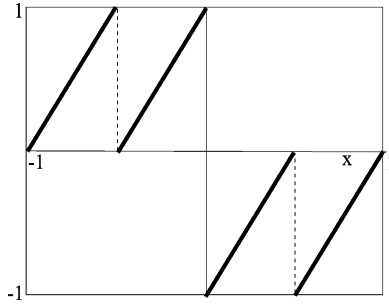


Fig. 3. The map considered in Example 10.

3.2. Eigenmeasures

For almost all x with respect to μ , the time-average of any function $f \in C(M)$ endowed with the sup norm can be represented as

$$f^*(x) = \int_M f \, d\mu_x,$$

where μ_x is an ergodic invariant measure for T [24]. The question that we investigate next is: are there objects on the phase space that can be used for a similar representation of the eigenfunctions f_ω^* ? We have the following definition [11]:

Definition 11. A complex-valued measure Φ that satisfies

$$\Phi(T^{-1}E) = e^{-i2\pi\omega} \Phi(E)$$

is called an eigenmeasure associated with eigenvalue $e^{-i2\pi\omega}$.

There is a direct way of defining eigenmeasures using harmonic averages, akin to the methods used in proving the ergodic decomposition theorem (as proved e.g. in [24]). Let $T : M \rightarrow M$ be as above. Let Σ_0^ω be the set of points on which the harmonic average f_ω^* exists for every continuous $f : M \rightarrow \mathbb{R}$. By the strong results of Wiener and Wintner [41] this set of measure one can be taken to be independent of ω . Let $C(M)$ be endowed with the sup norm. Note that $L_x^\omega : C(M) \rightarrow \mathbb{R}$ defined by

$$L_x^\omega f = f_\omega^*(x) = P_T^\omega f(x) = \lim_{n \rightarrow \infty} \frac{1}{n} \sum_{j=0}^{n-1} e^{i2\pi j\omega} f(T^j(x))$$

is a bounded linear functional. Thus, there exists a complex measure μ_x^ω such that

$$L_x^\omega f = f_\omega^*(x) = P_T^\omega(f)(x) = \int_M f \, d\mu_x^\omega,$$

for any $f \in C(M)$ [18]. Using continuity of T it can be shown that μ_x^ω is an eigenmeasure:

$$\int_M f \circ T \, d\mu_x^\omega(x) = L_x^\omega f \circ T = P_T^\omega(f \circ T)(x) = e^{-i2\pi\omega} P_T^\omega f(x) = e^{-i2\pi\omega} \int_M f \, d\mu_x^\omega.$$

3.3. The Perron–Frobenius operator

Similar to the case of invariant measures ([20], Theorem 4.1.1) eigenmeasures can be discussed in terms of the point-spectral properties of the Perron–Frobenius operator. In its most general form, the Perron–Frobenius operator is an operator on the space of Borel measures on M , defined by

$$P\mu = \mu \circ T^{-1},$$

and so

$$\int_A dP\mu = \int_{T^{-1}A} d\mu,$$

for any Borel set A . In the context of deterministic systems to avoid difficulties of working with measures that are singular we can define the Perron–Frobenius operator on the function space $L^1(M)$. Define the Perron–Frobenius operator $P : L^1 \rightarrow L^1$ adjoint to the Koopman operator $U : L^\infty \rightarrow L^\infty$ [20] by

$$\int_A Pf \, d\mu = \int_{T^{-1}A} f \, d\mu,$$

where μ is a Borel measure on M .

Proposition 12. Let Φ be a complex measure given by

$$\Phi(A) = \int_A g \, d\mu, \tag{6}$$

where $g \in L^1(M)$, A measurable. Then Φ is an eigenmeasure associated with the eigenvalue λ if and only if g is an eigenfunction of the Perron–Frobenius operator associated with the eigenvalue λ .

Proof. Let $g_\lambda \in L^1(M)$ be an eigenfunction associated with eigenvalue λ of P . Let a complex measure Φ be defined as in (6) with $g = g_\lambda$. Then

$$\Phi(T^{-1}A) = \int_M \chi_A \circ Tg_\lambda \, d\mu = \int_M \chi_A Pg_\lambda \, d\mu = \lambda \int_M \chi_A g_\lambda \, d\mu = \lambda\Phi(A).$$

Conversely, let Φ be an eigenmeasure given by (6) for some $g \in L^1(M)$. We know that $\Phi(T^{-1}A) = e^{-i2\pi\omega}\Phi(A) = \int_A e^{-i2\pi\omega}g \, d\mu$. But also $\Phi(T^{-1}A) = \int_M \chi_A \circ Tg \, d\mu = \int_M \chi_A Pg \, d\mu$ by the fact that $P : L^1 \rightarrow L^1$ and $U : L^\infty \rightarrow L^\infty$ are adjoint, and so

$$\int_M \chi_A e^{-i2\pi\omega}g \, d\mu = \int_M \chi_A Pg \, d\mu.$$

As this is valid for every Borel set A , we have that

$$Pg = e^{-i2\pi\omega}g,$$

and thus, g is an eigenfunction of P . □

If T preserves μ , $Pf = f \circ T^{-1}$ for invertible T . It is easy to show that if f_λ is an eigenfunction of U associated with the eigenvalue λ , then it is also an eigenfunction of P associated with eigenvalue $1/\lambda$ and vice versa. As P is unitary, it has the following property: if λ is an eigenvalue of P , then λ^{-1} is an eigenvalue of P . The same is valid for U . Thus, the point spectra of P and U are exactly the same. For ergodic T each of the eigenvalues is simple (i.e. the associated eigenspace is one-dimensional) [35]. Thus, the eigenvalues of P are also simple for ergodic T .

Definition 13. Let T be a transformation on M . The partition of M into level sets of an eigenfunction f_λ of U is called the λ -phase partition.

Clearly, the 0-phase partition is trivial (the whole set M can be taken as the only element of the partition) if T is ergodic. From the above analysis we get a very simple description of the phase space partitioning when T is ergodic. If there are no eigenvalues other than the simple eigenvalue at zero we can speak of *phase randomization*.

A study of the Perron–Frobenius operator in the context of eigenmeasures of stochastic systems that exhibit cycling behavior, was pursued in [11]. Additionally, in [10] eigenmeasures of interval exchange transformations were studied.

3.4. An example of harmonic analysis: the conservative case

Broer and Takens [5] studied the map $(x' = x + \omega_0, y' = y + x)$ on the unit torus that, as they show, has a mixed spectrum, i.e. the spectrum consists of a point part with eigenvalues $e^{-i2\pi n\omega_0}$, $n \in \mathbb{Z}$ and the associated eigenfunctions $e^{-i2\pi nx}$, $n \in \mathbb{Z}$ and a continuous part that is Lebesgue. The map is ergodic if ω_0 is irrational, but not mixing or even weakly mixing. It can be extended to a family of area-preserving maps T_a parametrized by the amplitude a :

$$\left. \begin{aligned} x' &= x + \omega_0 + a \sin(2\pi y) \\ y' &= y + x + a \sin(2\pi y) \end{aligned} \right\} \text{mod } 1.$$

A trajectory of the map T_0 , with $a = 0$, starting from $x = y = 0.3$ is shown in the Fig. 4. The orbit samples the phase space well, in accordance with the fact that the map is ergodic for that parameter value. In Fig. 5, we show numerically computed spectral information for the above map with $a = 0$, $\omega_0 = 1/(2\sqrt{2})$. As we mentioned, the properties of the spectrum are known analytically, but this case gives us a good validation point for our computations. In the top row of Fig. 5, we show on the left values of the function $f_1 = 0.25 \cos(2\pi x) + 0.25 \sin(2\pi y)$ on the trajectory shown in Fig. 4, for the first 100 iterates. This plot has a distinctly “stochastic” look. In the middle of the top row

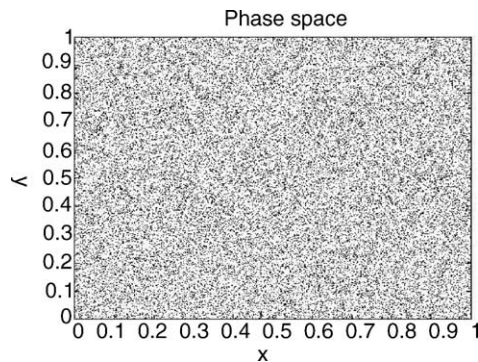


Fig. 4. Orbit of T_0 , starting from $x = y = 0.3$; 50,000 iterates.

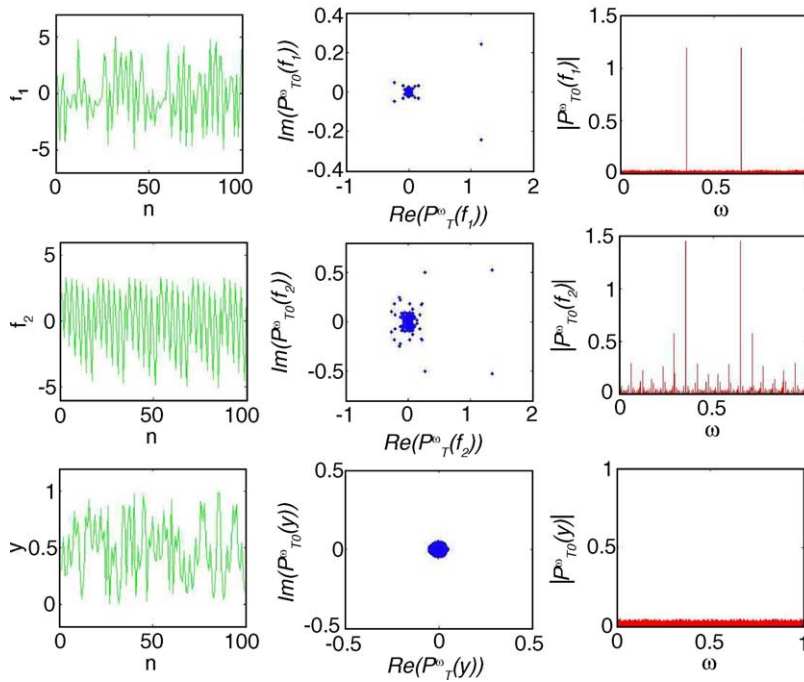


Fig. 5. Spectral properties of T_0 . See text for description.

of Fig. 5, we show values of the (complex valued) quantity

$$P_T^\omega f_1(x_0, y_0) = \frac{1}{N} \sum_{j=0}^{N-1} e^{i2\pi j\omega} f_1(T_0^j(x_0, y_0)).$$

The rightmost dot, on the real axis, represents the time average of the function, $f_1^*(x_0, y_0) = 0.5$. The two complex conjugate values farthest from the origin, at approximately $0.11 \pm i0.05$ correspond to $\omega = \pm 1/(2\sqrt{2})$. On the right of the top row of Fig. 4 we show $|P_T^\omega f_1(x_0, y_0)|$ as a function of ω . The computation is done over $N = 5000$ iterates, but the only thing that changes for larger N (we computed up to $N = 100,000$), is that all the values of $P_T^\omega f_1(x_0, y_0)$ shrink to zero, except for 0.5 and two complex conjugate values described above. In the top row rightmost figure, there are peaks present at ω_0 and $1 - \omega_0$ since the projection of f_1 to any eigenspace except for the ones at $e^{-i2\pi\omega_0}$, $e^{i2\pi\omega_0}$ is zero (note that we chose the horizontal axis in the top right figure to be $[0, 1)$ rather than $[-1/2, 1/2)$). Computation starting with different initial conditions and smaller number of iterates (down to about only 500) shows very similar features. Note the remarkable disparity between the aperiodic “appearance” of the signal and the spectrum that has a single clear peak. It is true that for the map in question, we know the importance of $\omega = 1/(2\sqrt{2})$ and its harmonics. However, the reader should imagine an unknown system with an observable producing the top left figure as its time trace. Computing the harmonic averages would identify the relevant frequency automatically.

In the second row, the same quantities are plotted for the function $f_2 = \tan(\cos(2\pi x/7)) - m$, where m is the mean of $\tan(\cos(2\pi x/7))$ on $[0, 1)$ (thus f_2 has mean zero on $[0, 1) \times [0, 1)$). The function f_2 does not depend on y and thus its behavior in time is quasiperiodic. The eigenvalues are of the form $e^{-i2\pi n\omega_0}$, and, in contrast with the first row, there are peaks in the rightmost plot of $|P_T^\omega f_2(x_0, y_0)|$ indicating several harmonics $n\omega_0$. This means that the function f_2 has non-zero projection onto eigenspaces of the Koopman operator that correspond to various n .

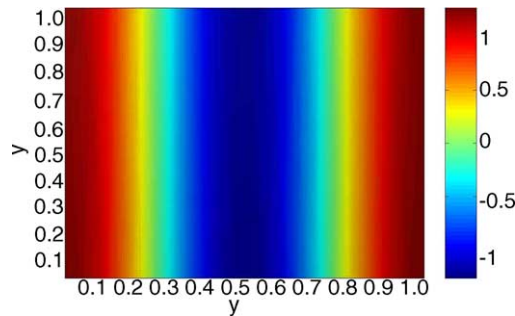


Fig. 6. Imaginary part of the harmonic average of f_1 under T_0 for $\omega = 1/(2\sqrt{2})$, taken over 10,000 iterates, on a grid of 40×40 initial conditions.

In the first and third plot of the third row we present iterates of the function y and its power spectral density. The function y does not contain any “rotation” by angle ω_0 and thus does not contain any distinguished peaks. More precisely, the projection of y to the space spanned by the eigenfunctions is 0. Of course, computationally, there is an error to this exact result and it is clear from the figure that it is of the order 10^{-3} for 5000 iterates. In the Fig. 6, we show the imaginary part of the harmonic average $P_{T_0}^{\omega_0} f_1$ for $\omega_0 = 1/(2\sqrt{2})$, taken over 10,000 iterates, on a grid of 40×40 initial conditions. We know that this function is in the linear span of $\cos(2\pi x)$ and $\sin(2\pi x)$ and the calculation confirms this. Note that despite the fact that the dynamical system is ergodic for $a = 0$, we can (partially) tell where the trajectory came from by computing its phase. Of course, we cannot tell the initial y but horizontal initial conditions are distinguished.

Next we consider the case $a = 0.01$. A trajectory of the map $T_{0,0.01}$ starting from $x = y = 0.3$ is shown in the Fig. 7. Appearance of islands is clear from this figure, but there is still a single large zone in the phase space that appears to be ergodic. In this case, the spectrum of a trajectory starting in the ergodic zone changes only slightly from the case $a = 0$, as shown in the Fig. 8. The ordering of plots is the same as in the Fig. 5. In the Fig. 9, we show the imaginary part of the harmonic average $P_{T_0}^{\omega_0} 10 f_1$ for $\omega_0 = 1/(2\sqrt{2})$, taken over 50,000 iterates, on a grid of 400 initial conditions. The computation is much harder in this case, due to the coupling in the system, but features of the eigenfunction are clearly close to the case $a = 0$, with the exception of isolated zones corresponding to islands in the Fig. 7. We computed harmonic averages for $10 f_1$ instead of f_1 just to get a better contrast in the plot – of course, the resulting harmonic average is just a constant (10) multiple of the one that would be obtained by computing harmonic average of f_1 . We also performed some smoothing over frequencies ω , in the range $[0.3535, 0.3545]$ -

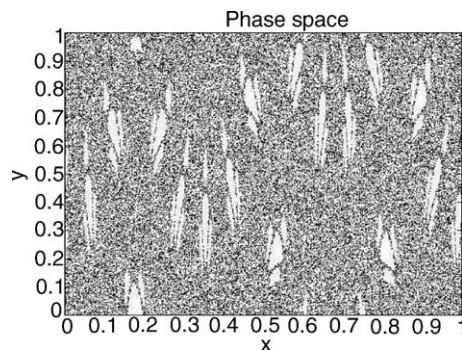


Fig. 7. Orbit of $T_{0,0.01}$, starting from $x = y = 0.3$; 100,000 iterates.

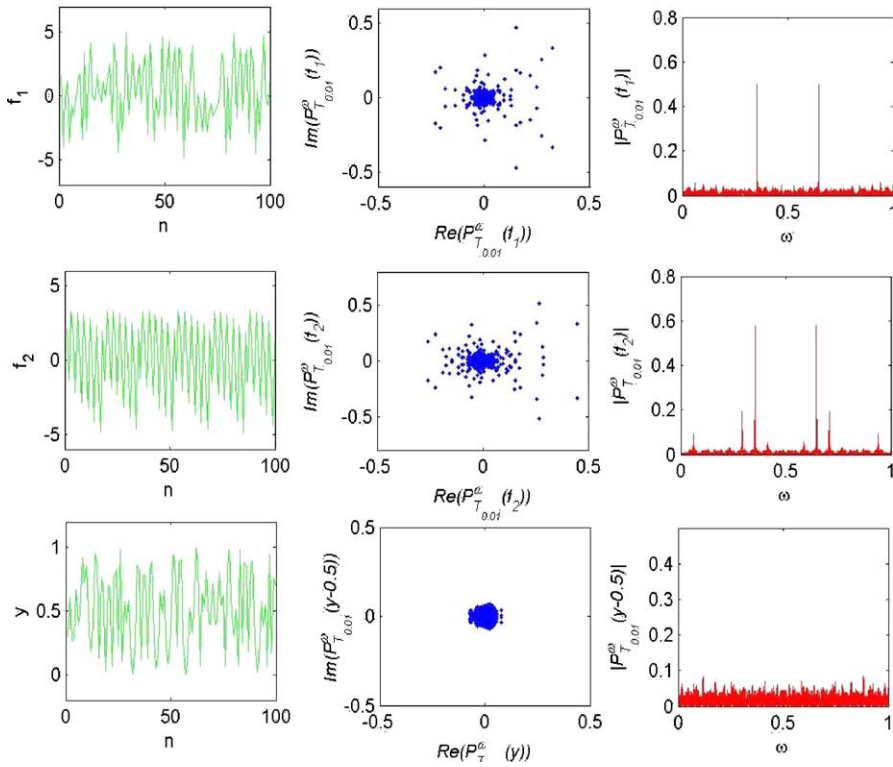


Fig. 8. Spectral properties of $T_{0.01}$. See text for description.

one has to remember that we are computing highly non-smooth quantities. For the case $a = 0$ this was not necessary due to the nice convergence properties.

In the Fig. 10, we show the plot equivalent to those in Figs. 5 and 8, computed for 25,000 iterates with $a = 0.5$. In this case, $P_{T_{0.5}}^{\omega}(f)$ evaluated at the point $(0.3, 0.3)$ becomes smaller and smaller in the range of the number of iterates up to $N = 25,000$. The phase seems to be randomized outside of the island that exists in the phase-space plot at the upper left corner.

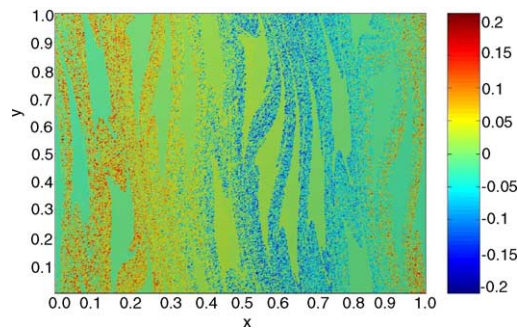


Fig. 9. Imaginary part of the harmonic average of $10f_1$ under $T_{0.01}$ for $\omega = 1/(2\sqrt{2})$, taken over 50,000 iterates, on a grid of 400×400 initial conditions.

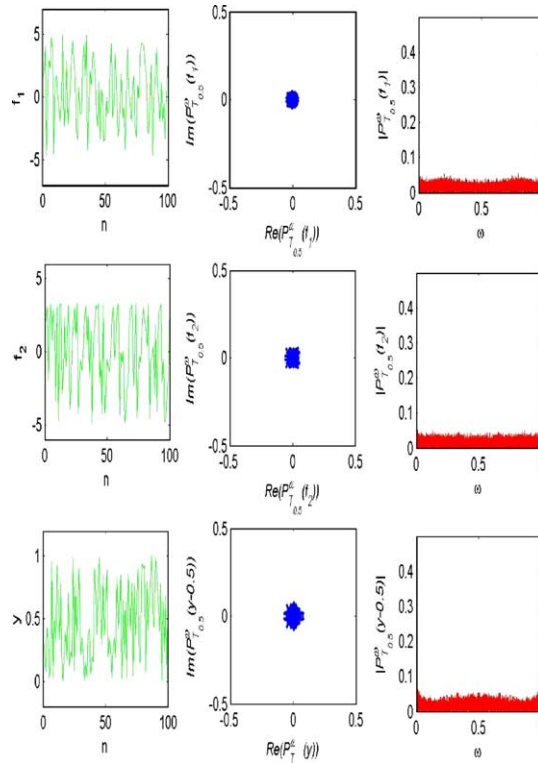


Fig. 10. Spectral properties of $T_{0.5}$. See text for description.

3.5. Examples of harmonic analysis: the dissipative case

In this subsection, we present examples of the use of above harmonic analysis ideas for dissipative maps on a torus. First we consider the following simple map:

$$\left. \begin{aligned} x' &= \gamma(x - \omega_0) + \omega_0 \\ y' &= y + x \end{aligned} \right\} \text{mod } 1. \tag{7}$$

Under assumption that ω_0 is irrational and $0 < \gamma < 1$, the above map has an invariant circle at $x = \omega_0$, on which the dynamics is given by irrational rotation $y = y + \omega_0$ (see Fig. 11b where a trajectory of the map (7) with $\omega_0 = 0.5613245623$, starting at $x_0 = 0.8, y_0 = 0.2$ is shown). In Fig. 11a, we show the contour plot of the argument of the complex eigenfunction obtained by taking the harmonic averages with $\omega = \omega_0$ of the function $g = \cos(2.5 \cos(2\pi y)) + 2.5 \sin(2\pi x)$ over the trajectories of the map. In particular, we know that the eigenfunction can be written as $r \exp(2\pi\theta(x_0, y_0))$, where r is the (constant) modulus (note that the map is ergodic with respect to the delta measure concentrated on the invariant circle at $x = \omega_0$, and thus any eigenfunction has constant modulus). In Fig. 11a, we plot contour plot of $\theta(x_0, y_0)$. All the points of the same straight skewed line contour have the same "asymptotic phase", i.e. their trajectory asymptotically approaches the trajectory of the point that is on the intersection of that line and $x = \omega_0$. Note that the eigenspace at $\lambda = \exp(2\pi\omega_0)$ is two-dimensional, but the λ -partition is accurately represented by $\theta(x_0, y_0)$. Next, consider the following dissipative perturbation of an integrable

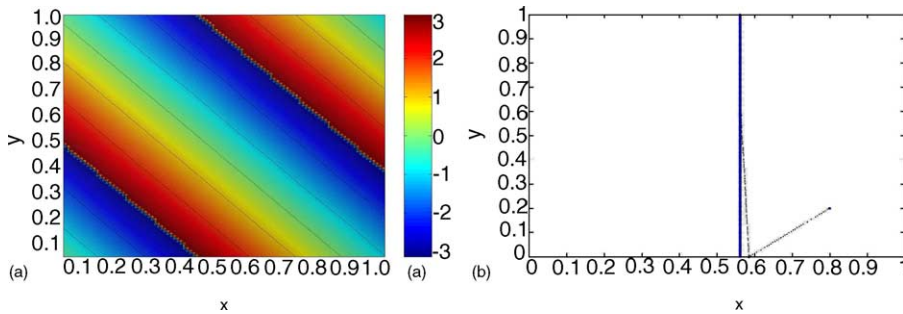


Fig. 11. (a) Angle of the harmonic average of g under map (7) for $\omega = \omega_0 = 0.5613245623$, taken over 1000 iterates, on a grid of 30×30 initial conditions. (b) Trajectory of the map (7) with $\omega = \omega_0 = 0.5613245623$, starting at $x_0 = 0.8, y_0 = 0.2$.

twist map:

$$\left. \begin{aligned} x' &= (1 - \gamma)x + a \sin^2(2\pi y) \\ y' &= y + x + a \sin(2\pi y) \end{aligned} \right\} \text{mod } 1. \tag{8}$$

where $\gamma = 0.06123456756432, a = 0.03$. For sufficiently small a , it can be shown that there is an invariant circle close to $x = 0.25$ (see Fig. 12b where a trajectory of the map (8) starting at $x_0 = 0.8, y_0 = 0.2$ is shown). In Fig. 12a, we show the contour plot of the argument of the complex eigenfunction obtained by taking the harmonic averages at $\omega = 0.245$ of the function $g = \cos(2.5 \cos(2\pi y) + 2.5 \sin(2\pi x))$ over the trajectories of the map. Clearly, the “asymptotic phase” for this map has much more complicated distribution than that in the previous example. Harmonic partitions can be obtained from embedded data as well, i.e. when we do not have ability to measure the full state of the system. In Fig. 13, we show the imaginary part of the finite-time harmonic average of $f_1 + f_2 + f_3 + f_4$ from Example 2. In particular, we show contour plot visualizing the level sets of finite time average $f_{1,\omega}^{*,N} + f_{2,\omega}^{*,N} + f_{3,\omega}^{*,N} + f_{4,\omega}^{*,N}$, where

$$f_{1,\omega}^{*,N} = \frac{1}{N} \sum_{j=1}^N \exp(2\pi i j \omega) \sin(2\pi \theta^j) \sin(2\pi \theta^{j-1}),$$

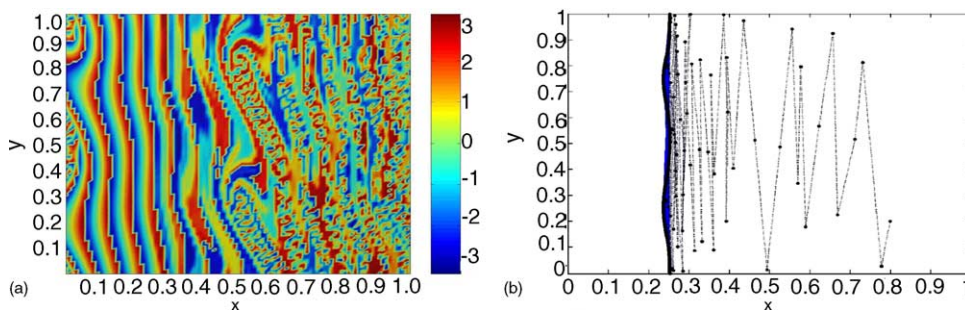


Fig. 12. (a) Angle of the harmonic average of g under map (8) for $\omega = 0.245$, taken over 1000 iterates, on a grid of 30×30 initial conditions. (b) Trajectory of the map (8) with $\gamma = 0.06123456756432, a = 0.03$, starting at $x_0 = 0.8, y_0 = 0.2$.

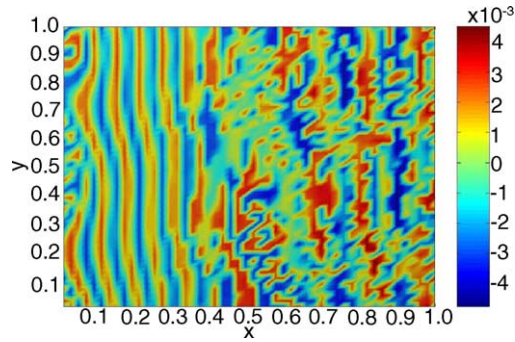


Fig. 13. (a) Imaginary part of the harmonic average of $f_1 + f_2 + f_3 + f_4$ under map (8) for $\omega = 0.245$, taken over 5000 iterates, on a grid of 50×50 initial conditions.

$$f_{2,\omega}^{*,N} = \frac{1}{N} \sum_{j=1}^N \exp(2\pi i j \omega) \sin(2\pi 3 \theta^j) \cos(2\pi 3 \theta^{j-1}),$$

$$f_{3,\omega}^{*,N} = \frac{1}{N} \sum_{j=1}^N \exp(2\pi i j \omega) \sin(2\pi 5 \theta^j) \cos(2\pi 5 \theta^{j-1}),$$

$$f_{4,\omega}^{*,N} = \frac{1}{N} \sum_{j=1}^N \exp(2\pi i j \omega) \cos(2\pi 8 \theta^j) \sin(2\pi 8 \theta^{j-1}),$$

4. Stochastic systems

The above theory can be extended to stochastic systems. We will present the application of the above ideas to a stochastic system in the next section and we provide the theoretical framework and relevant results here.

4.1. Introduction and set-up

For our purpose, the most convenient context in which to analyze stochastic systems is that of Random Dynamical Systems (RDS) [2]. We will work with the Discrete Random Dynamical System (DRDS)

$$x_{i+1} = T(x_i, \xi_i), \quad \xi_{i+1} = S(\xi_i), \quad y_i = f(x_i) \quad (9)$$

where $i \in \mathbb{Z}$, $x \in M$ a compact Riemannian manifold, $\xi = \{\dots, \xi^{-1}, \xi^0, \xi^1, \dots\} \in N^{\mathbb{Z}}$, i.e. $\xi^j \in N$, where N is a compact Riemannian manifold endowed with a probability measure p that is absolutely continuous with respect to the Lebesgue measure on N . The product space $N^{\mathbb{Z}}$ is endowed with the standard product measure Ω . S is the shift transformation $S\{\dots, \xi^{-1}, \xi^0, \xi^1, \dots\} = \{\dots, \xi^0, \xi^1, \xi^2, \dots\}$. We consider observables $f : M \rightarrow \mathbb{R}$ or \mathbb{C} , $f \in L^1(M)$. We denote $T_\xi^i(x) = T_{\xi^{i-1}} \circ \dots \circ T_{\xi^0}$ where $T_{\xi^j}(x) = T(x, \xi^j)$. We assume that $T_\xi(x)$ is C^r , $r \geq 1$ in x for every $\xi \in N$. With some abuse of notation, we will call the above DRDS T (note that T denotes a family of transformations indexed over ξ , rather than any particular superposition). A probabilistic measure μ on M endowed with the Borel sigma algebra is invariant for measurable T iff

$$\mathbb{E}[\mu(T^{-1}(B, \xi))] = \mu(B)$$

for every measurable B where $\mathbb{E}[\mu(T^{-1}(B, \xi))] = \int_{N^{\mathbb{Z}}} \mu(T^{-1}(B, \xi)) d\Omega(\xi)$. The analogue of the Koopman operator is the *stochastic Koopman operator* U_s defined by

$$U_s f(x) = \mathbb{E}[f \circ T(x, \xi)],$$

where $\mathbb{E}[f \circ T(x, \xi)] = \int_{N^{\mathbb{Z}}} f \circ T(x, \xi) d\Omega(\xi)$. The *expectation of the time-average of f* under T is given by

$$\mathbb{E}f^*(x) = \lim_{n \rightarrow \infty} \frac{1}{n} \sum_{i=0}^{n-1} U_s^i f(x). \tag{10}$$

The partition of M into level sets of $\mathbb{E}f^*$ is denoted by ζ_f . An ergodic measure on M is an invariant measure μ such that $\mathbb{E}f^*(x) = \int_M f(x) d\mu(x)$ a.e. on M for every $f \in L^1(M)$. The ergodic partition ζ_e of M under T is a partition into sets D_α such that on each set D_α there exists an ergodic measure μ_{D_α} and its properties are equal to the situation described for the deterministic case in the [Appendix A.1](#).

4.2. Ergodic partitions and invariant measures

To state results equivalent to [Theorem 2](#) we need to use a stochastic version of the Takens embedding theorem. This has recently been provided in [\[37\]](#) (see e.g. [Theorem 7](#) there). In particular, assume that N is a compact manifold and p absolutely continuous with respect to the Lebesgue measure on N . For generic, C^r , $r \geq 1$ pairs (f, T) and almost every $\xi \in N^{\mathbb{Z}}$, the map $e : M \rightarrow \mathbb{R}^{2m+1}$ given componentwise by $e(x) = (f(x), f(T_\xi x), f(T_\xi^2 x), \dots, f(T_\xi^{2m} x))$ is an embedding and thus $e(M)$ is a compact submanifold of \mathbb{R}^{2m+1} . Again, it is then necessarily contained in a sufficiently large box \mathbb{B} of side length $l_\xi > 2 \cdot \max_x |f(x)|$ centered at the origin of \mathbb{R}^{2m+1} . We can regard \mathbb{B} as a torus \mathbb{T}^{2m+1} , i.e. the embedding e can be regarded as a map $e : M \rightarrow \mathbb{T}^{2m+1}$.

Theorem 14. *Let M be a compact Riemannian manifold of dimension m and N a compact manifold of dimension n endowed with a measure p that is absolutely continuous with respect to the Lebesgue measure on N . Let $\kappa_i, i \in \mathbb{N}$ be a sequence of continuous periodic functions in $C([-l_\xi/2, l_\xi/2])$ that is complete. Consider a countable set of functions $f_{i_1, \dots, i_{2m+1}} = \kappa_{i_1}(f) \cdot \kappa_{i_2}(f \circ T_\xi) \cdot \dots \cdot \kappa_{i_{2m+1}}(f \circ T_\xi^{2m})$ where $i_1, i_2, \dots, i_{2m+1} \in \mathbb{N}$. Then, for almost every ξ , for $C^r, r \geq 1$ pairs (f, T) it is a generic property that the ergodic partition of a $C^r, r \geq 1$ DRDS T on M is*

$$\zeta_e = \bigvee_{i_1, \dots, i_{2m+1}} \zeta_{f_{i_1, \dots, i_{2m+1}}}.$$

The proof of this theorem closely resembles the steps taken in the deterministic case. The Markov property of the DRDS allows for the use of ergodic partition technique provided by Yosida [\[42\]](#). The stochastic version of the Takens embedding theorem proven as [Theorem 7](#) in [\[37\]](#) is used.

4.3. Harmonic analysis

The family of operators $\mathbb{E}P_T^\omega$,

$$\mathbb{E}P_T^\omega(f) \equiv \mathbb{E}f_\omega^* = \lim_{n \rightarrow \infty} \frac{1}{n} \sum_{j=0}^{n-1} e^{i2\pi j\omega} U_s^j f,$$

plays the role analogous to the family P_T^ω in the deterministic case. In particular, a nonzero $\mathbb{E}P_T^\omega$ is the orthogonal projection operator onto the eigenspace of U_s associated with the eigenvalue $e^{-i2\pi\omega}$ (see the first remark on pg.

215 in [42]). It is interesting to discuss *deterministic factors* of random dynamical systems. A deterministic factor of a DRDS T on $A \subset M$ is a map $S : B \rightarrow B$ such that there is a measurable *factor map* (or homomorphism) $F : A \rightarrow B$, $\mathbb{E}(F \circ T) = S \circ F$ a.e. and $\mu(F^{-1}(E)) = \nu(E)$ for all measurable E and measures μ, ν , where T preserves μ and S preserves ν . Assume that T is ergodic on A with an invariant ergodic measure μ_A . We have the following:

Theorem 15. *Let T be an invertible DRDS, $h_\omega : A \rightarrow \mathbb{C}$ be a non-constant eigenfunction of U_S associated with the eigenvalue $e^{-i2\pi\omega}$. Then h_ω is a factor map and T has a factor that is a rotation on a circle by an angle $-2\pi\omega$. Conversely, if T admits a factor map to rotation on the circle by an angle $2\pi\omega$ then there is an eigenfunction of T associated with eigenvalue $e^{-i2\pi\omega}$.*

We provide the proof in the [Appendix A.1](#) since it is in spirit the same as in the deterministic case, but differs in a variety of technical issues.

Corollary 16. *Let A be a set in the ergodic partition of T . $\mathbb{E}P_T^\omega(f)$ is not constant on A for every $f : M \rightarrow \mathbb{C}$ if and only if T has a factor that is a rotation on the circle by an angle $2\pi\omega$.*

We can now define eigenmeasures as complex measures Φ that satisfy $\mathbb{E}(\Phi(T(E, \xi_0))) = e^{-i2\pi\omega}\Phi(E)$. The complex measure defined by $\Phi(E) = \mathbb{E}P_T^\omega(\chi_E)$ is clearly an eigenmeasure. The stochastic Perron–Frobenius operator $P_S : L^1 \rightarrow L^1$ can be defined by

$$\int_C P_S f(x) d\mu(x) = \mathbb{E} \int_A f \cdot (\chi_C \circ T(x, \xi)) d\mu(x),$$

for $f \in L^1(A)$. It is easy to see that the operator P_S is adjoint to the stochastic Koopman operator. The connection between the eigenvalues of P_S and eigenmeasures is the same as in the deterministic case:

Proposition 17. *Let Φ be a complex measure given by*

$$\Phi(E) = \int_E g d\mu, \tag{11}$$

where $g \in L^1(M)$. Then Φ is an eigenmeasure associated with the eigenvalue λ if and only if g is an eigenfunction of the stochastic Perron–Frobenius operator associated with the eigenvalue λ . We call g_λ the charge density.

The proof follows the lines of the deterministic case and we omit it.

Example 18. Consider a DRDS given by

$$x^{i+1} = -1 \cdot \Theta(\xi^i), \quad \xi^{i+1} = S\xi^i, \tag{12}$$

where $x \in [-1, 1]$, $\xi \in [0, 1]^{\mathbb{N}}$, $\Theta(\xi^i) = \xi_0^i$, where ξ_0^i is the value of the sequence $\xi^i = \{\dots, \xi_{-n}^i, \dots, \xi_{-1}^i, \xi_0^i, \xi_1^i, \dots, \xi_n^i, \dots\}$ at index 0, and the probability measure p is the Lebesgue measure on $[0, 1]$. The factor map for (12) is given by $F : [-1, 1] \rightarrow \{-1, 1\}$, $F(x) = -1$ if $x \in [-1, 0]$, $F(x) = 1$ if $x \in (0, 1]$. The deterministic factor is $G(a) = -a$, where $a \in \{-1, 1\}$.

The above example is in some sense canonical: from the proof of [Theorem 15](#) in the [Appendix A.1](#), it is clear that the random process moves points from a level set of an eigenfunction with modulus 1 to another level set of the same eigenfunction, with probability 1.

This completes our discussion of discrete random dynamical systems. The system (9) can be also regarded as a control system (see e.g. [12,40]). When we consider ξ as a control input, the whole ergodic partition on $M \times N^{\mathbb{Z}}$ becomes an interesting object to study. For the discussion of invariant measures in this direction, see e.g. [2].

Now we turn to practical considerations. The concepts defined above allow us to propose procedures for identification of parameters of complex nonlinear systems. We discuss these methods and apply them to experimental data from a combustion experiment in the next section.

5. Identification of parameters of nonlinear complex systems

We believe that the ideas introduced above can be turned into a practical tool for analyzing and modeling the behavior of dynamical systems with complex dynamics. The whole formalism is based on data from a single observable and, in contrast to previous uses of Takens' theorem recovers statistical information linked to geometrical properties of the attractor instead of the purely geometrical information. In this section, we use them to analyze and estimate parameters for a model of an experimentally studied combustion process. In the next subsection, we review the methods that are usually used in such analysis and connect them with the methods that we have developed here. We apply the new procedures to the experimental data in Section 5.2.

5.1. Probability histograms

The rigorous results proven above suggest that we should take time-averages of a complete set of continuous functions to study properties of invariant measures. In applications such as analysis of experimental data, what is typically available is probability histograms. Here, we show that these involve a similar construction to the one provided above, a composition of (discontinuous!) functions $\kappa_j : \mathbb{R} \rightarrow \mathbb{R}$ with an observable $g : M \rightarrow \mathbb{R}$.

In the context of chaotic dynamical systems the probabilistic approach is often taken and a system is described in terms of a histogram of a specific function g on the phase space. Let b be the bin size for the histogram and $z_j \in \mathbb{R}$, $j \in \mathbb{Z}$ a sequence of numbers such that $z_{j+1} = z_j + b$. By the histogram we mean a step function, constant on every interval $I_j = (z_j - b/2, z_j + b/2]$:

$$H_g^T(I_j, x) = \lim_{n \rightarrow \infty} \frac{1}{n} \sum_{i=0}^{n-1} \kappa_j \circ g(T^i(x)) = \kappa_j^*(x),$$

where $x \in M$. $H_g^T(I_j, x)$ tells us the proportion of time the time-series spends in the interval I_j . The function κ_j is the characteristic function on the interval $I_j = (z_j - b/2, z_j + b/2]$, i.e. $\kappa_j(u) = 1$ if $z_j - b/2 < u \leq z_j + b/2$ and zero otherwise. If T is ergodic, H is the same function for almost every initial condition x . A possible pseudometric for ergodic systems would be

$$d(T_1, T_2) = \sum_j [H_g^{T_1}(I_j) - H_g^{T_2}(I_j)]^2,$$

where the sum is over some finite set of j 's.

The lesson learned from the rigorous study is that we should take time-averages (i.e. histograms) of products of $(\kappa_j \circ g(T^i(x)))$ where $i = 0, \dots, 2m$, and include them into the pseudometric. The appropriate experimental procedure would be to: (1) get the data from observable g ; (2) determine the dimensionality m of the system using the appropriate embedding theorem; (3) formulate the model of the same dimension; (4) form histograms of products of $\kappa_j \circ g(T^i(x))$ for experiment and model; (5) compare these histograms in some metric.

Example 19. Probability histograms for correlated processes. As mentioned above, one of the common ways of comparing behavior of two systems with complex behavior is taking histograms for a single observable. To show the dangers of this approach when the dynamics of the system is not completely decorrelated and usefulness of the Lemma 21 in this context, consider two systems having limit cycle attractors in the delay phase space shown in Fig. 14. Both of the limit cycles are elliptical, one of them having its major axis aligned with the axis z_1 , the other with z_2 . The dynamics on both limit cycles is assumed to be symmetric with respect to both z_1 and z_2 axis and thus the probability histogram of f (denoted by $p(f)$ in Fig. 14) is the same for both systems. However, let κ_+ be the indicator function on the interval $(0, l)$. Then $\kappa_+(f) \cdot \kappa_+(f \circ T)$ is the indicator function for the upper right quadrant

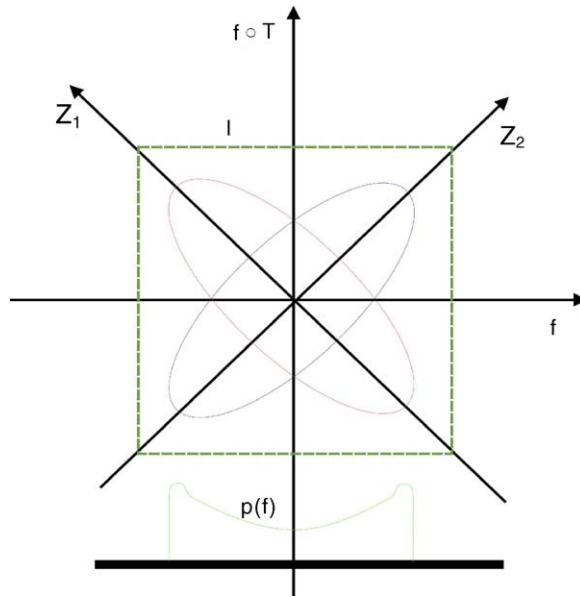


Fig. 14. An example in which two different limit cycles give the same histogram of f .

of the box of side l shown in the Fig. 14. Clearly, the amount of time that these two systems spend in the upper right quadrant is different and thus the time average of this product function reveals the difference in the invariant measures supported on the limit cycles.

We can also define spectral histograms by considering $P_T^\omega(\kappa_j) = (\kappa_j)_\omega^*$. Histograms in the case of stochastic processes are defined similarly.

5.2. An example: Identification of parameters of a combustion model with noise

In this section, we present an example of using the formalism developed above to optimize parameters of a model describing a United Technologies Research Center (UTRC) 4MW single-nozzle combustion rig operating close (in parameter space) to instability associated with a lean condition, i.e., with low value of fuel to air ratio ([19]). This was done in a non-automatized manner, by trial-and-error search for the best parameters due to computing-time limitations induced by the number of parameters. Of course, an automatized procedure could in principle be designed based on the above considerations on pseudometrics. There are several points we wanted to make in this example. One is that the method is quite sensitive to change of parameters of the model and easily distinguishes, for example, between a limit cycling and a stable noisy system. Another is that phase information is important even in noisy processes. Namely, the data studied here exhibits harmonic averages consistent with the process being close to one with a deterministic factor.

A simple model of a combustion process is an interconnection of a linear acoustic model and nonlinear heat release model that consists of a delay and a saturation function. The system is driven by broad-band stochastic disturbance. More precisely, a discrete-time model equations used to simulate pressure oscillations in the UTRC combustion rig were

$$\begin{aligned} x_{i+1}^1 &= (-\alpha + \cos(\omega_0 T_s))x_i^1 - \sin(\omega_0 T_s)x_i^2, \\ x_{i+1}^2 &= \sin(\omega_0 T_s)x_i^1 + (-\alpha + \cos(\omega_0 T_s))x_i^2 + K_3 h(K_2 x_{i-N}^1) + K_1 n_i, \end{aligned} \quad (13)$$

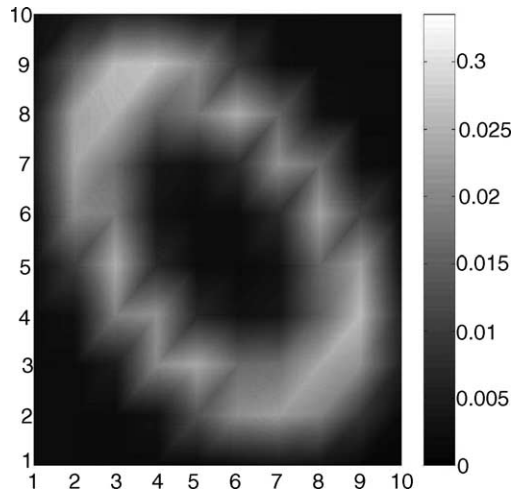


Fig. 15. Time average plot for indicator functions from experimental data.

where $T_s = 0.0005$, $\omega_0 = 2\pi f_0$, $K_3 = 0.0525$, and h is a saturation function defined as $h(u) = u$ for $-s < u < s$, $h(u) = -s$ for $u \leq -s$, and $h(u) = s$ for $s \leq u$. Variables x_i^1 , x_i^2 are unsteady components of pressure in the combustor at two different times, while variable n_i represents noise. The model was implemented in Simulink. To simulate noise, a Simulink model of a band-limited white noise with power 0.01 was used. Note that the model described by (13) is a Discrete Random Dynamical System (DRDS) of the type that was studied in Section 4. We choose a two-dimensional embedding space for the system.

To obtain the harmonic averages 20,000 samples (10 s sampled at 2 kHz) of experimentally obtained combustor pressure and pressure from Simulink model simulations were used. The experimental data presents a spectrum with a single peak at about $f = 207$. We examined the results of harmonic analysis results for a range of model parameters lead by this spectral information. Values of f_0 , N , α , K_2 , s , and K_1 were varied until a good agreement between harmonic averages of results of simulations and experimental data was found. A good fit to experimental data was obtained for parameters $f_0 = 207$, $N = 10$, $\alpha = 0.03$, $K_2 = 2000$, $s = 5$, $K_1 = 0.0788$.

Let $p(i)$ be the vector of two subsequent values of the pressure at times $(l+1)/20000$, $l/2000$ obtained from experimental data or the model. Figs. 15 and 16 we show the plot of time-averages

$$\chi_{(i,j)}^* = \frac{1}{20000} \sum_{i=1}^{20000} \chi_{(i,j)}(p(i))$$

of indicator functions $\chi_{(i,j)}$ on squares defined in the embedding space (an indicator function is 1 if a point is inside the square of side length l and 0 elsewhere). A grid of 10×10 indicator functions was used with $l = 2$ psi, their time-averages computed and assigned to nodes labelled (i, j) where i, j vary from 1 to 10 (for this approach to experimental data analysis and discussion of related distance functions, see [29]). The results shown in 15, for the experimental data and 16 for the model that we found a good fit to the data are, for the sake of better visualization, linearly interpolated shaded contour-plots of the time-averages. To show the sensitivity of the model (in the sense that some model parameters produce very poor approximation to experimental data) we show in the Fig. 17 the time averages for the case of model parameters being $f_0 = 207$, $N = 9$, $\alpha = 0.03$, $K_2 = 2000$, $s = 5$, $K_1 = 0.0788$.

In Fig. 18, we show the absolute value of the difference between the time average of indicator functions obtained from experimental data and that obtained from model that is deemed a good representation for the experimental data. The values are an order of magnitude smaller than the values presented in Figs. 15 and 16. Thus, the approximation error is about 10%. In the Fig. 19, we show the absolute value of the difference between the time average of indicator

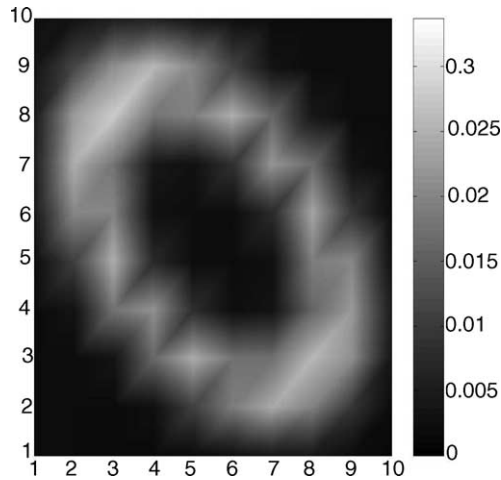


Fig. 16. Time averages for indicator functions for model with parameters that provide a good match with the experimental data.

functions obtained from experimental data and that obtained from model that is deemed a bad representation for the experimental data. The model error in that case is of the same order of magnitude as the data itself.

Using the developed methods of data analysis it is relatively easy to distinguish systems that exhibit noisy limit cycles from those exhibiting stable, lightly damped behavior with noise (in our case a system possessing a spiral-node fixed point). In Fig. 20, we show (on top) both the spectrum of signals from experimental data (blue) and stable, lightly damped model (red) for model parameters: $f_0 = 207$, $N = 10$, $\alpha = 0.03$, $K_2 = 9.52$, $s = 15$, $K_1 = 0.0788$. It is clear that while the spectra are very similar, the probability density functions shown in the bottom plot show a strong difference.

While the difference of the limit cycling and stable lightly damped system is clear already from the probability density function, we investigate it in the context of the tools developed in the theory part of the paper. In Fig. 21 we show the plot of the time averages of indicator functions presented in the same fashion as those in Figs. 15

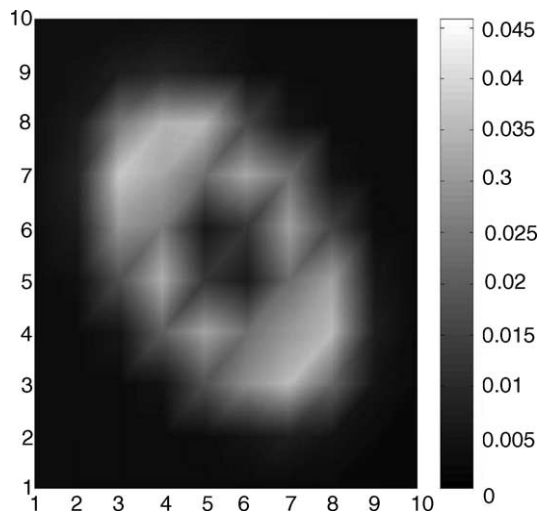


Fig. 17. Time averages for indicator functions for model with parameters that provide a poor match for the experimental data.

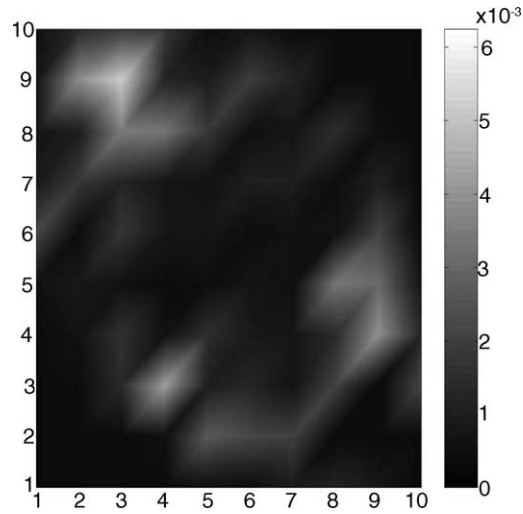


Fig. 18. Absolute value of the difference between the time averages for experimental data and the model with parameters corresponding to good fit.

and 16. The nature of the distribution of the time-averages is clear: there is a peak centered at the box (5, 5); this is where the stationary point of the underlying stable lightly damped deterministic system (with $K_1 = 0$ in (13)) is.

It is interesting to also examine the phase information provided by experimental data and different models in the context of the theory provided above. In Figs. 22–24, we present contour plots of the absolute value of harmonic averages

$$\chi_{\omega(i,j)}^* = \frac{1}{20000} \sum_{i=1}^{20000} e^{i2\pi j\omega} \chi_{\omega(i,j)}(p(i))$$

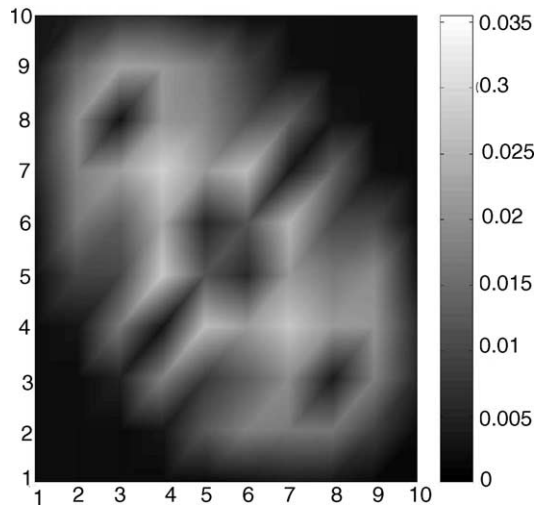


Fig. 19. Absolute value of the difference between the time averages for experimental data and the model with parameters corresponding to poor fit.

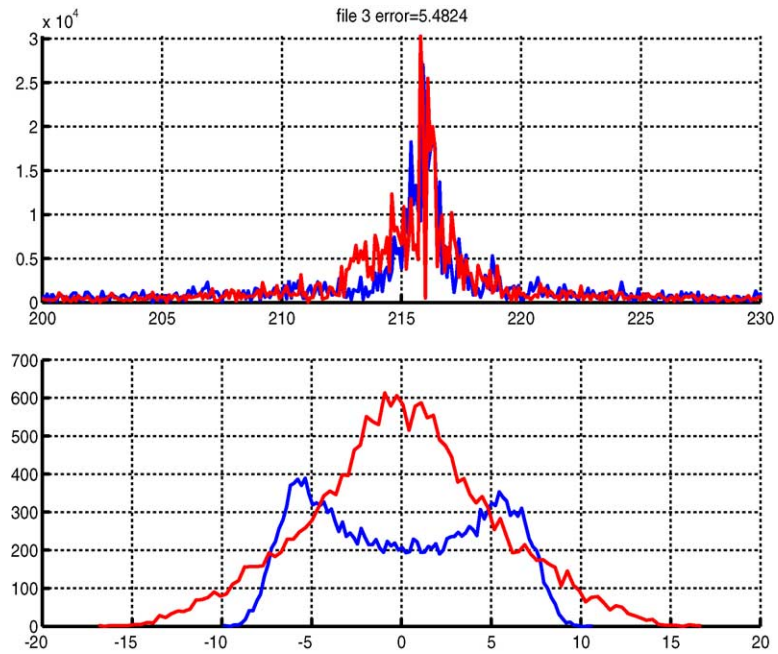


Fig. 20. Top: spectrum of experimental data (blue) and stable, lightly damped, noisy model (red). Bottom: probability density functions of the signal for experimental data (blue) and stable, lightly damped, noisy model (red). (For interpretation of the references to color in this figure legend, the reader is referred to the web version of the article.)

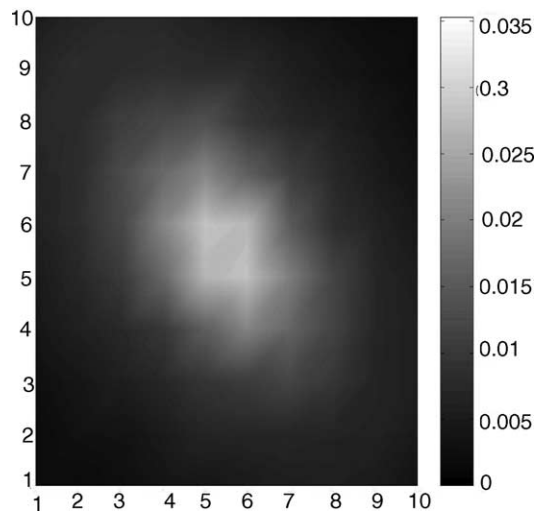


Fig. 21. Plot of the time averages of indicator functions for the stable, lightly damped noisy model of the experimental data.

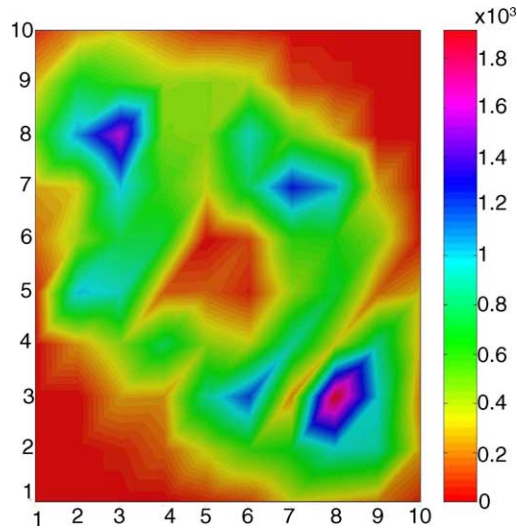


Fig. 22. Contour plot of the harmonic averages of indicator functions for frequency corresponding to the peak obtained from the experimental data.

obtained at the frequency ω where the experimental data and models (“good fit” limit cycling model and stable lightly damped model) have a peak. While both the plot from the experimental data in Fig. 22 and from the “good fit” model in Fig. 23 have well-defined features around the geometric location of the noisy limit cycle, the plot obtained from the stable, lightly damped model at the same frequency is comparatively featureless – as shown in Fig. 24. This is to be expected, given that in limit cycling system with noise the factor analysis provided in Section 4 suggests existence of a non-uniform signed measure such that the average of density of the measure over boxes (i, j) is approximated by the harmonic averages. This density is concentrated at the location of the limit cycle. In the stable lightly damped model, the phase is “randomized” - there is no factor and no “true” cycling in the system.

It is also worth pointing out that by taking the “wrong” model obtained by setting $x_1 \rightarrow -x_1$ (reflection across x_2 axis) and using the parameters of the “good fit” limit cycling model we obtain a model whose 1– dimensional probability density plot matches that of the experimental data, shown in blue in Fig. 20 while the two-dimensional plot of time averages shows Fig. 16 reflected across x_2 axis, thus exhibiting behavior described in Example 19.

In [22], the question of characterization of limit cycling instability in jet engine combustors was investigated. The classical method of PDF analysis was used in conjunction with the Takens embedding theorem to provide such characterization. The methods we exhibited here, that use the new, statistical version of the Takens theorem are suitable for taking such a study further, to the realm of model parameter identification and model validation, the importance of which in the context of combustion processes was indicated in [17].

5.3. Effect of finite data sets and finite sets of functions

The data analysis method that we propose requires analysis of a basis of functions on the phase space (our functions κ_i) whose statistical properties are analyzed starting from a finite-time data set. If the trajectory of a system is time-periodic or quasi-periodic, the harmonic averages will converge at a rate $1/n$ where n is the number of data points (for discussion of this simple fact and a specific application, see [26]). When the trajectory is in a chaotic zone, and the system is strongly mixing, convergence will typically be of the order $1/\sqrt{n}$ and therefore quite slow.

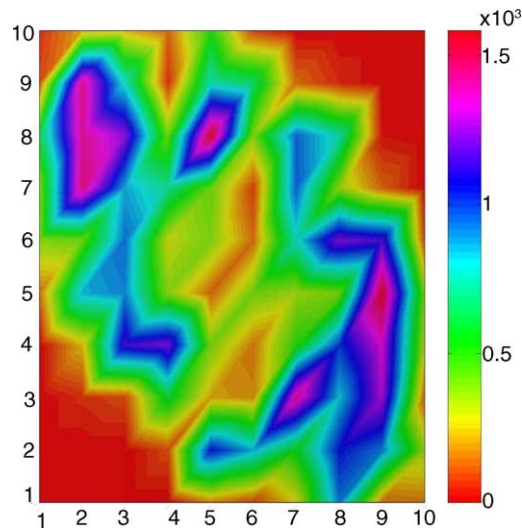


Fig. 23. Contour plot of the harmonic averages of indicator functions for frequency corresponding to the peak obtained from the "good fit" limit cycling model.

The choice of different functions κ_i will determine the "spatial" (i.e. phase space) scale of comparison of systems. For example, wavelet bases can be employed to detect spatially localized features of a system such as high order resonances in the standard map [21]. In the example presented in this section it is the interplay between the time-scale of the data and spatial scale of the feature in the phase space that determines the spatial scale of the functions κ_i used.

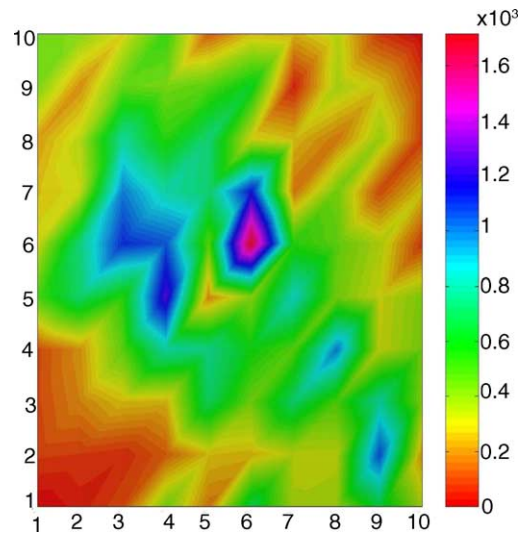


Fig. 24. Contour plot of the harmonic averages of indicator functions for frequency corresponding to the peak obtained from the stable, lightly damped noisy model.

6. Conclusions

In this paper, we presented some ideas that serve as a framework within which model validation and analysis of nonlinear and/or stochastically driven systems can be done.

Practitioners of experimental and numerical analysis of dynamical systems have found great use of Takens embedding theorem type results. But, embedding methods are often supplemented by statistical considerations such as analysis of probability density functions and spectral analysis. This is especially the case when data is polluted by noise. Here, we linked Takens embedding type results with ergodic theory analysis to provide an ergodic–theoretic understanding of probability density and spectral data, both for deterministic and random dynamical systems.

Following the premise that time averages of certain functions on the phase space of a system can be easily obtained experimentally, while complete invariant measures are hard to observe, we have studied the relationship between the two. We have also argued that invariant measures *do not* describe (even in the sense of statistics) everything we would like to know about the asymptotic dynamics of systems. We introduced a family of operators on the space of functions and discussed how the question about the difference of asymptotic dynamics can be transformed into a question on the behavior of this family of operators. Based on this, we introduced pseudometrics on the space of dynamical systems that split this space into equivalence classes of systems having the same (in the sense of the chosen pseudometric) asymptotic dynamics. We presented an example in which this formalism is used to optimize parameters of a model of a combustion experiment. As opposed to much of the previous work in this direction, our interest lies not in getting the correct short-term (relative to the time-scales of the problem) prediction but getting the correct long-time trends – in terms of geophysics, we are not interested in weather prediction but in the climate.

We stress that questions of identification or validation of asymptotic properties of nonlinear finite-dimensional systems with complex dynamics are in this approach transferred to questions of identification or validation of a linear, albeit infinite-dimensional Koopman operator. Our hope is that some of the methods developed in control theory of linear systems can be used to study these issues further.

On the practical side, we provided a constructive method for obtaining relevant statistics from experiments. This method depends on a *choice* of a particular complete set of periodic functions on an interval. While this choice is irrelevant from the perspective of the theory, as *any* choice of a complete set will give *all* of the required statistical information, the practical issues arising from this are numerous. For example: which complete set do we choose in order to obtain approximate (finite data, finite set of functions) results that are optimal in some sense? We hope to resolve some of these questions in future studies.

Acknowledgments

We would like to thank Alexandre Chorin, Richard Montgomery and John Hauser for useful discussions. Andre Valente carefully read the manuscript and suggested various improvements. During part of the work on this paper, I.M. was at the Division of Engineering and Applied Sciences, Harvard University, Cambridge, MA. I.M. was partially supported by an AFOSR grant 98-1-0146, AFOSR grant F49620-98-C-0006 and the Sloan Fellowship. AB was supported by AFOSR grants F49620-01-C-0021 and FA9550-04-C-00442.

Appendix A

A.1. Ergodic partition of a dynamical system

Ergodic partition ζ_e of M under T is a partition into sets D_α such that on each set D_α there exists an ergodic measure μ_{D_α} such that

- (1) $\mu_{D_\alpha}(D_\alpha) = 1$,
- (2) for every $f \in L^1(M)$, $f^*(x \in D_\alpha) = \int_{D_\alpha} f \, d\mu_{D_\alpha}$ a.e. with respect to μ_{D_α} and
- (3) for any invariant measure μ , and any measurable set B ,

$$\mu(B) = \int_M \mu_{D_\alpha(x)}(B) \, d\mu(x),$$

where $D_\alpha(x)$ is the element of the partition such that $x \in D_\alpha$.

A.2. Proof of Theorem 2

The proof relies on two lemmas. The first one extends a standard argument in ergodic theory which says that the ergodic partition is partition into joint level sets of time averages of a countable, dense set of continuous functions (for the proof and applications see [25,27]) to allow for taking only joint level sets of time averages of a complete set of functions. The second lemma tells us how to generate such a complete set of functions using only one observable.

Lemma 20. *Let M be a compact metric space and $T : M \rightarrow M$ a C^r , $r \geq 1$, diffeomorphism. Assume there exist a complete system of functions $\{f_i\}$, $f_i \in C(M)$, $i \in \mathbb{N}^+$ i.e. finite linear combinations of f_i are dense in $C(M)$. The ergodic partition of a C^r , $r \geq 1$ diffeomorphism $T : M \rightarrow M$ on M is*

$$\zeta_e = \bigvee_{i \in \mathbb{N}^+} \zeta_{f_i}. \tag{A.1}$$

Proof. It can be shown (see [25,27]) that $\zeta_e = \bigvee_{f \in S} \zeta_f$, where S is any countable dense set in $C(M)$. Note that finite linear combinations over rationals of functions f_i form a dense, countable set S_{f_i} in $C(M)$. The partition induced by this set of functions,

$$\zeta = \bigvee_{i \in \mathbb{N}^+} \zeta_{f_i}.$$

is clearly the same as $\bigvee_{f \in S_{f_i}} \zeta_f$. □

Lemma 21. *Let M be a compact Riemmanian manifold of dimension m , $T : M \rightarrow M$ a C^r , $r \geq 1$ diffeomorphism, f a real C^r function on M and κ_i , $i \in \mathbb{N}$ a sequence of continuous periodic functions in $C([-l/2, l/2])$ that is complete. Then, for pairs (f, T) it is a generic property that finite linear combinations over rationals of the sequence of functions $\kappa_{i_1}(f) \cdot \kappa_{i_2}(f \circ T) \cdot \dots \cdot \kappa_{i_{2m+1}}(f \circ T^{2m})$ (where $i_1, i_2, \dots, i_{2m+1} \in \mathbb{N}^+$ are dense in $C(M)$).*

Proof. By Takens embedding theorem [38,37], for generic (f, T) the map $e : M \rightarrow \mathbb{R}^{2m+1}$ given componentwise by

$$e(x) = (f(x), f(Tx), f(T^2x), \dots, f(T^{2m}x))$$

is an embedding and thus $e(M)$ is a compact submanifold of \mathbb{R}^{2m+1} . It is then necessarily contained in a sufficiently large box \mathbb{B} of side length l centered at the origin of \mathbb{R}^{2m+1} . We can regard \mathbb{B} as a torus \mathbb{T}^{2m+1} , i.e. the embedding e can be regarded as a map $e : M \rightarrow \mathbb{T}^{2m+1}$. The embedding e is a diffeomorphism between M and $e(M)$, and thus for any continuous $h : M \rightarrow \mathbb{R}$, $g = h \circ e^{-1} : e(M) \rightarrow \mathbb{R}$ is a continuous function. By Tietze extension theorem g admits an extension to a continuous function \tilde{g} defined on \mathbb{B} . The functions $\kappa_{i_1}(\pi_1) \cdot \kappa_{i_2}(\pi_2) \cdot \dots \cdot \kappa_{i_{2m+1}}(\pi_{2m+1})$, where π_i is the i th coordinate function, $\pi_i(\mathbf{x}) = x_i \in \mathbb{R}$, constitute a complete set in $C(\mathbb{B})$ [36] and thus finite linear

combinations over rationals of these functions are dense in $C(\mathbb{B})$. In particular, for any ϵ we can find a finite number of rational $c_{i_1 i_2 \dots i_{2m+1}}$ such that

$$|\tilde{g} - \sum c_{i_1 i_2 \dots i_{2m+1}} \kappa_{i_1} \cdot \kappa_{i_2} \cdot \dots \cdot \kappa_{i_{2m+1}}| = \max_{y \in \mathbb{T}^{2m+1}} |\tilde{g}(y) - \sum c_{i_1 i_2 \dots i_{2m+1}} \kappa_{i_1} \cdot \kappa_{i_2} \cdot \dots \cdot \kappa_{i_{2m+1}}(y)| < \epsilon.$$

But this implies

$$\begin{aligned} g \circ e - \sum c_{i_1 i_2 \dots i_{2m+1}} \kappa_{i_1}(f) \cdot \kappa_{i_2}(f \circ T) \cdot \dots \cdot \kappa_{i_{2m+1}}(f \circ T^{2m}) \\ \geq \max_{x \in M} |h(x) - \sum c_{i_1 i_2 \dots i_{2m+1}} \kappa_{i_1}(f(x)) \cdot \kappa_{i_2}(f \circ T(x)) \cdot \dots \cdot \kappa_{i_{2m+1}}(f \circ T^{2m}(x))| < \epsilon. \end{aligned}$$

Because h is an arbitrary continuous function and ϵ is arbitrarily small, we are done. □

Theorem 2 is thus proven.

A.3. Proof of Theorem 15

First observe that the expectation of the modulus of h_ω is constant a.e. with respect to an invariant measure as

$$\int_A \mathbb{E}(|h_\omega| \circ T_\xi) d\mu_A = \mathbb{E} \int_A (|h_\omega| \circ T_\xi) d\mu_A = \int_A |h_\omega| d\mu_A.$$

by invariance of μ_A . In addition, $\mathbb{E}(|h_\omega| \circ T_\xi) = \mathbb{E}(|h_\omega \circ T_\xi|) \geq |\mathbb{E}(h_\omega \circ T_\xi)| = |e^{-i2\pi\omega} h_\omega| = |h_\omega|$. It follows that $|h_\omega| = \mathbb{E}(|h_\omega| \circ T_\xi)$ a.e. and thus the modulus of h_ω is constant a.e. as T is ergodic on A .

Lemma 22. *Let h_ω be an eigenfunction associated with the eigenvalue $e^{-i2\pi\omega}$ of U_S . Then $h_\omega \circ T_\xi(x) = e^{-i2\pi\omega} h_\omega(x)$ for almost every $\xi \in N$.*

Proof. Assume not. We have

$$U_S h_\omega(x) = \mathbb{E} h_\omega \circ T_\xi(x) = e^{-i2\pi\omega} h_\omega(x).$$

Since $|h_\omega|$ is constant on A , without loss of generality, we assume $|h_\omega| = 1$. Thus

$$|\mathbb{E} h_\omega \circ T_\xi(x)| = \left| \int_N h_\omega \circ T_\xi(x) d\Omega(\xi) \right| \leq \int_N |h_\omega \circ T_\xi(x)| d\Omega(\xi) = 1.$$

Equality holds iff $h_\omega \circ T_\xi(x)$ is constant for almost every ξ . But since we know

$$|\mathbb{E} h_\omega \circ T_\xi(x)| = |e^{-i2\pi\omega} h_\omega(x)| = 1,$$

we get a contradiction with the assumption that $h_\omega \circ T_\xi(x)$ is not constant for almost every ξ . □

Corollary 23. *For any measurable $E \subset S^1$, for an eigenfunction h_ω associated with the eigenvalue $e^{-i2\pi\omega}$ of U_S , we have*

$$\mu_A \{x \in A | \mathbb{E} h_\omega \circ T_\xi(x) \in E\} = \mu_A \{x \in A | h_\omega \circ T_\xi(x) \in E\}, \tag{A.2}$$

for almost every $\xi \in N$.

Proof. Let $C = \{x \in A | \mathbb{E}h_\omega \circ T_\xi(x) \in E\}$, $D_\xi = \{x \in A | h_\omega \circ T_\xi(x) \in E\}$. Assume there is a set $F \subset N$, $\Omega(F) > 0$ such that $\mu_A(D_\xi) \neq \mu_A(C)$ for every $\xi \in F$. Consider the set $G = \{(x, \xi) \in (A \times N) | \xi \in F, x \in (C/D_\xi)\}$. Clearly, $(\mu_A \times \Omega)(G) > 0$ and this contradicts the fact that, by Lemma 22 for every $x \in C$, for almost every $\xi \in N$, we have $h_\omega \circ T_\xi(x) \in E$. \square

Proof (Proof of Theorem 15). Without loss of generality we assume that $|h_\omega| = 1$. Define the *angle variable* (see [42], pg. 392) $\theta(x)$ by $h_\omega(x) = e^{-i2\pi\theta(x)}$. We have

$$\mathbb{E}(h_\omega \circ T_\xi) = e^{-i2\pi\omega} h_\omega = e^{-i2\pi\omega} e^{-i2\pi\theta(x)} = e^{-i2\pi(\theta(x)+\omega)}.$$

Thus, it is clear that $\mathbb{E}(h_\omega \circ T_\xi) = S \circ h_\omega$ where S the rotation by an angle $-2\pi\omega$ on a circle of radius 1. Now define a measure ν on the circle by $\nu(E) = \mu_A(h_\omega^{-1}(E))$ where μ_A is the ergodic measure for T . We get

$$\nu(S^{-1}(E)) = \mu_A(h_\omega^{-1} \circ S^{-1}(E)) = \mu_A((S \circ h_\omega)^{-1}(E)) = \mu_A((\mathbb{E}h_\omega \circ T_\xi)^{-1}(E))$$

Now by Corollary 23 we have

$$\mu_A((\mathbb{E}h_\omega \circ T_\xi)^{-1}(E)) = \mathbb{E}\mu_A((h_\omega \circ T_\xi)^{-1}(E)) = \mathbb{E}\mu_A(T_\xi^{-1} \circ h_\omega^{-1}(E)) = \mu_A(h_\omega^{-1}(E)) = \nu(E).$$

The converse is clear by the following construction: let $h : M \rightarrow S^1$ be a factor map such that the factor of T is a clockwise rotation by an angle $2\pi\omega$. Then

$$\mathbb{E}(h(T_\xi x)) \cdot h^{-1}(x) = e^{i2\pi\omega},$$

and h is an eigenfunction associated with eigenvalue $e^{-i2\pi\omega}$. \square

References

- [1] H.D.I. Abarbanel, Analysis of Observed Chaotic Data, Springer-Verlag, New York, 1996.
- [2] L. Arnold, H. Crauel, Random dynamical systems, Springer-Verlag, Lect. Notes Math. 1486 (1991) 1–22.
- [3] B. Bamieh, M. Dahleh, Energy amplification in channel flows with channel excitation, Phys. Fluids 13 (2001) 3258–3269.
- [4] G. Berkooz, An observation on probability density equations, or when do simulations reproduce statistics? Nonlinearity 7 (1994) 313–328.
- [5] H. Broer, F. Takens, Mixed spectra and rotational symmetry, Arch. Rational Mech. Anal. 124 (1993) 13–42.
- [6] K.M. Butler, B.F. Farrell, Three-dimensional optimal perturbations in viscous shear flow, Phys. Fluids A 4 (1992) 1637.
- [7] A.J. Chorin, O.H. Hald, R. Kupferman, Non-markovian optimal prediction, Monte Carlo Meth. And Appl. 7 (2001) 99–109.
- [8] P. Cvitanović, R. Artuso, P. Dahlquist, R. Mainieri, G. Tanner, G. Vattay, N. Whelan, A. Wirzba, Classical and Quantum Chaos, 2001, unpublished lecture notes.
- [9] D. D’Alessandro, I. Mezić, M. Dahleh, Statistical properties of controlled fluid flows with applications to control of mixing, Syst. Controls Lett. 45 (2002) 249–256.
- [10] M. Dellnitz, G. Froyland, S. Sertl, On the isolated spectrum of the Perron–Frobenius operator, Nonlinearity 13 (2000) 1171–1188.
- [11] M. Dellnitz, O. Junge, On the approximation of complicated dynamical behavior, SIAM J. Numer. Anal. 36 (2) (1999) 491–515.
- [12] F. Colonius, W. Kliemann, Lyapunov exponents of control flows, Springer-Verlag, Lect. Notes Math. 1486 (1991) 1–22.
- [13] G. Froyland, K. Judd, A.I. Mees, K. Murao, D. Watson, Constructing invariant measures from data, Int. J. Bifurcat. Chaos 5 (4) (1995) 1181–1192.
- [14] A. Garulli, C. Mocenni, A. Tesi, A. Vicino, Integrating identification and qualitative analysis for the dynamic model of a lagoon, Int. J. Bifurcat. Chaos 13 (2003).
- [15] L.H. Gustavsson, Energy growth of three-dimensional disturbances in plane Poiseuille flow, J. Fluid Mech. 224 (1991) 241.
- [16] P. Halmos, Approximation theories for measure-preserving transformations, Trans. Am. Math. Soc. 55 (1943) 1–18.
- [17] J. Harper, C. Johnson, Y. Neumeier, T. Lieuwen, B. T. Zinn, Flame response to flow disturbances in a gas turbine combustor, 2001, AIAA paper AIAA-01-0486.

- [18] E. Hewitt, K. Stromberg, *Real and Abstract Analysis*, Springer-Verlag, New York, 1965.
- [19] C.A. Jacobson, A.I. Khibnik, A. Banaszuk, J. Cohen, W. Proscia. Active control of combustion instabilities in gas turbine engines for low emissions. Part I. Physics-based and experimentally identified models of combustion instability. Applied Vehicle Technology Panel Symposium on Active Control Technology, Braunschweig, Germany, 2000.
- [20] A. Lasota, M.C. Mackey, *Chaos, Fractals and Noise*, Springer-Verlag, 1994.
- [21] Z. Levnajić I. Mezić. Visualization of dynamical systems using harmonic analysis, 2004, UCSB preprint.
- [22] T.C. Lieuwen, Experimental investigation of limit-cycle oscillations in an unstable gas-turbine combustor, *J. Propulsion Power* 18 (2002) 61–67.
- [23] A.J. Majda, I. Timofeyev, E.V. Eijnden, Models for stochastic climate prediction *Proc. Natl. Acad. Sci.*, 96 (1999) 14687–14691.
- [24] R. Mane, *Ergodic Theory and Differentiable Dynamics*, Springer-Verlag, 1987.
- [25] I. Mezić. On geometrical and statistical properties of dynamical systems: theory and applications, PhD thesis, California Institute of Technology, 1994.
- [26] I. Mezić, F. Sotiropoulos, Ergodic theory and experimental visualization of invariant sets in chaotically advected flows, *Phys. Fluids* 14 (7) (2002) 2235–2243.
- [27] I. Mezić, S. Wiggins, A method for visualization of invariant sets of dynamical systems based on the ergodic partition, *Chaos* 9 (1999) 213–218.
- [28] K. Mischaikow, M. Mrozek, J. Reiss, A. Szymczak, Constructing of symbolic dynamics from experimental time series, *Phys. Rev. Lett.* 82 (6) (1999) 1144–1147.
- [29] R. Moeckel, B. Murray, Measuring the distance between time series, *Physica D* 102 (1997) 187–194.
- [30] K. Petersen, *Ergodic Theory*, Cambridge University Press, Cambridge, 1995.
- [31] S.C. Reddy, D.S. Henningson, Energy growth in viscous channel flows, *J. Fluid Mech.* 252 (1993) 209.
- [32] V.A. Rokhlin, Selected topics from the metric theory of dynamical systems, *Amer. Math. Soc. Transl. Series 2*, (49) (1966) 171–240.
- [33] R. Saravanan, J.C. McWilliams, Stochasticity and spatial resonance in interdecadal climate fluctuations, *J. Climate* 10 (1997) 2299–2320.
- [34] T. Sauer, J.A. Yorke, M. Casdagli, *Embedology*, *J. Statist. Phys.* 65 (1991) 579–616.
- [35] Ya.G. Sinai, *Topics in Ergodic Theory*, Princeton University Press, 1994.
- [36] I. Singer, *Bases in Banach Spaces I*, Springer-Verlag, New York, 1970.
- [37] J. Stark, D.S. Broomhead, M.E. Davies, J. Huke, Takens embedding theorems for forced and stochastic systems, *Nonlinear Anal.*, 30 (1997) 5303–5314.
- [38] F. Takens, Detecting strange attractors in turbulence, Springer-Verlag, *Lect. Notes Math.* 898 (1981) 368–381.
- [39] L.N. Trefethen, A.E. Trefethen, S.C. Reddy, T.A. Driscoll, Hydrodynamic stability without eigenvalues, *Science* 261 (1993) 578.
- [40] U. Vaidya, I. Mezić, Controllability for a class of area-preserving twist maps, *Physica D* 189 (2004) 234–246.
- [41] N. Wiener, A. Wintner, Harmonic analysis and ergodic theory, *Am. J. Math.* 63 (1940).
- [42] K. Yosida, *Functional Analysis*, Springer-Verlag, New York, 1980.